iScience

CellPress
OPEN ACCESS

Article

Regulation of Gluconeogenesis by Aldo-keto-reductase 1a1b in Zebrafish

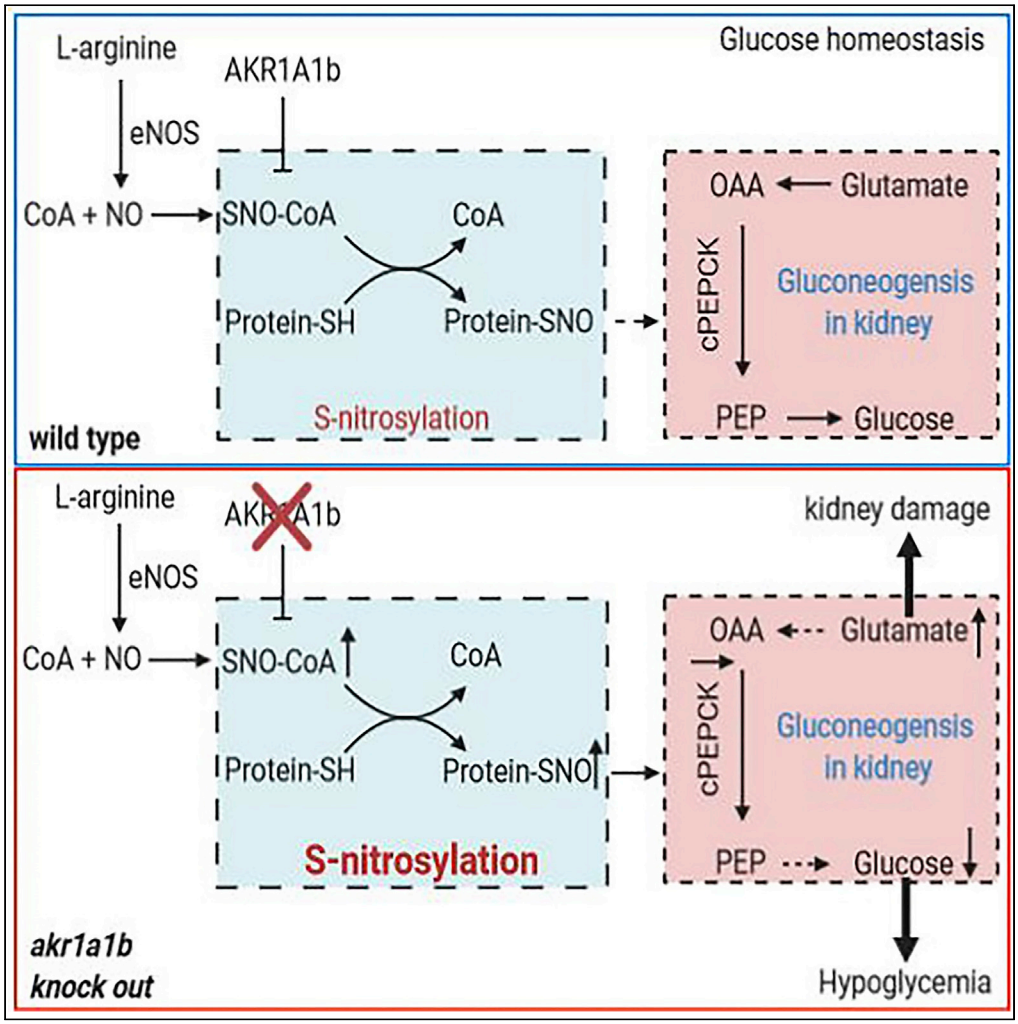

Xiaogang Li, Felix Schmöhl, Haozhe Qi, ..., Thomas Fleming, Peter Paul Nawroth, Jens Kroll

jens.kroll@medma.uni-heidelberg.de

HIGHLIGHTS

Adult *akr1a1b*$^{-/-}$ mutant zebrafish develop fasting hypoglycemia

Loss of Akr1a1b inhibits renal phosphoenolpyruvate carboxykinase (PEPCK) expression

Accumulation of glucogenic amino acid glutamate alters the kidney in *akr1a1b* mutants

Akr1a1b regulates gluconeogenesis via protein-S-nitrosylation

Li et al., iScience *23*, 101763
December 18, 2020
https://doi.org/10.1016/j.isci.2020.101763

iScience

CellPress
OPEN ACCESS

Article

Regulation of Gluconeogenesis by Aldo-keto-reductase 1a1b in Zebrafish

Xiaogang Li,[1] Felix Schmöhl,[1] Haozhe Qi,[1] Katrin Bennewitz,[1] Christoph T. Tabler,[1] Gernot Poschet,[2] Rüdiger Hell,[2] Nadine Volk,[3] Tanja Poth,[4] Ingrid Hausser,[5] Jakob Morgenstern,[6] Thomas Fleming,[6] Peter Paul Nawroth,[6,7,8] and Jens Kroll[1,9,*]

SUMMARY

Regulation of glucose homeostasis is a fundamental process to maintain blood glucose at a physiological level, and its dysregulation is associated with the development of several metabolic diseases. Here, we report on a zebrafish mutant for Aldo-keto-reductase 1a1b (*akr1a1b*) as a regulator of gluconeogenesis. Adult *akr1a1b*$^{-/-}$ mutant zebrafish developed fasting hypoglycemia, which was caused by inhibiting phosphoenolpyruvate carboxykinase (PEPCK) expression as rate-limiting enzyme of gluconeogenesis. Subsequently, glucogenic amino acid glutamate as substrate for gluconeogenesis accumulated in the kidneys, but not in livers, and induced structural and functional pronephros alterations in 48-hpf *akr1a1b*$^{-/-}$ embryos. *Akr1a1b*$^{-/-}$ mutants displayed increased nitrosative stress as indicated by increased nitrotyrosine, and increased protein-S-nitrosylation. Inhibition of nitrosative stress using the NO synthase inhibitor L-NAME prevented kidney damage and normalized PEPCK expression in *akr1a1b*$^{-/-}$ mutants. Thus, the data have identified Akr1a1b as a regulator of gluconeogenesis in zebrafish and thereby controlling glucose homeostasis.

INTRODUCTION

Regulation of glucose homeostasis is a fundamental process to maintain blood glucose at a physiological level. Glucose is a major energy substrate for several organs, which includes but is not limited to the brain and red blood cells, and dysregulation of glucose homeostasis can lead to several metabolic diseases, such as diabetes, obesity, dyslipidemia, and cardiovascular diseases. Blood glucose concentrations are determined by the glucose uptake from the intestine, glucose-metabolizing or -producing pathways, and hormones including insulin and glucagon. Major glucose-depriving pathways are glycolysis, glycogenesis, and lipogenesis, whereas glucose-producing pathways are glycogenolysis and gluconeogenesis (Alsahli and Gerich, 2017; Petersen et al., 2017).

Gluconeogenesis produces glucose and uses mainly lactate, glycerol, or glucogenic amino acids, including alanine and glutamate as substrates (Yip et al., 2016). It has long been postulated that the liver is the sole source of glucose generation, but this hypothesis was disapproved by observations that the mammalian renal cortical tissue can make gluconeogenesis *in vitro*, in animals and in humans (Benoy and Elliott, 1937; Bergman and Drury, 1938; Bjorkman et al., 1979; Drury et al., 1950). Interestingly, later studies have identified a substrate preference for gluconeogenesis in the liver for alanine, whereas the kidney prefers glutamate (Stumvoll et al., 1999). Gluconeogenesis shows a reciprocal regulation with glycolysis and is regulated on different levels. One regulation relates to glucagon-induced gene expression of key regulating enzymes phosphoenolpyruvate carboxykinase (PEPCK) and glucose-6-phosphatase, whereas allosteric regulation of fructose-1,6-bisphosphatase is mediated by fructose-2,6-bisphosphate, AMP, and ADP. Increasing evidence supports the hypothesis that the kidney plays a vital role in glucose homeostasis via gluconeogenesis, especially in the prolonged fasting state. Aberrant renal gluconeogenesis is associated with the development of type 2 diabetes mellitus (Bjorkman et al., 1980; Meyer et al., 2002), and increased renal glucose release by up to 300% in patients with type 2 diabetes mellitus have been reported (Meyer et al., 1998). Thus, renal gluconeogenesis is essential for glucose homeostasis in physiology.

[1]Department of Vascular Biology and Tumor Angiogenesis, European Center for Angioscience (ECAS), Medical Faculty Mannheim, Heidelberg University, Mannheim 68167, Germany

[2]Metabolomics Core Technology Platform, Centre for Organismal Studies, Heidelberg University, Heidelberg 69120, Germany

[3]Tissue Bank of the National Center for Tumor Diseases (NCT), Heidelberg 69120, Germany

[4]CMCP - Center for Model System and Comparative Pathology, Institute of Pathology, University Hospital Heidelberg, Heidelberg 69120, Germany

[5]Electron Microscopy Lab, Institute of Pathology, University Hospital Heidelberg, Heidelberg 69120, Germany

[6]Department of Internal Medicine I and Clinical Chemistry, Heidelberg University Hospital, Heidelberg 69120, Germany

[7]German Center for Diabetes Research (DZD), München-Neuherberg 85764, Germany

[8]Joint Heidelberg-IDC Translational Diabetes Program, Helmholtz-Zentrum, München, Heidelberg 69120, Germany

[9]Lead Contact

*Correspondence: jens.kroll@medma.uni-heidelberg.de

https://doi.org/10.1016/j.isci.2020.101763

Akr1A1 belongs to the Aldo-keto reductase (Akr) superfamily, which has a function in the reduction of carbonyl-containing compounds to their corresponding alcohols (Singh et al., 2015). One additional prominent member of the family is Akr1b1, which regulates in addition to its carbonyl-detoxifying function glucose homeostasis by converting glucose into sorbitol (Brownlee, 2001). Recent data have identified a function for mouse Akr1A1 acting as an S-nitroso-CoA reductase. *Akr1a1* knockout mice displayed increased protein-S-nitrosylation and were protected from acute kidney injury, which was mediated by balancing glycolysis by regulating the S-nitrosylation of pyruvate kinase M2 (Zhou et al., 2019).

Different from other animals, two separate *akr1a1* genes exist in zebrafish, namely, *akr1a1a* and *akr1a1b*, whose functions have not been studied yet. The zebrafish has been established as a model for diabetes research in the past decade (Heckler and Kroll, 2017; Jorgens et al., 2015; Lodd et al., 2019; Lou et al., 2020; Schmohl et al., 2019; She et al., 2018; Wiggenhauser et al., 2020), because glucose homeostasis in zebrafish is very similar to that humans and other mammals and alterations in glucose homeostasis are associated with organ damage, including the kidney, eyes, and nerves (Olsen et al., 2010). Therefore, this study aimed to generate an *akr1a1b* knockout animal model and evaluate the function of Akr1a1b in glucose homeostasis and organ function in embryonic, larval, and adult zebrafish. The study has identified Akr1a1b as a regulator of gluconeogenesis and shows how altered gluconeogenesis damages the kidney.

RESULTS

Expression of *akr1a1b* in Zebrafish and Generation and Validation of *akr1a1b*$^{-/-}$ Mutants

Previous studies showed *akr1a1* expression in virtually every tissue in human and mice (Fagerberg et al., 2014; Yue et al., 2014), with the highest expression being in the kidney tubular system (Scotcher et al., 2016). Yet, the expression of *akr1a1b* in zebrafish has not been analyzed. Thus, we investigated early developmental stages from 24 to 120 hours post fertilization (hpf) and organs from adult zebrafish for *akr1a1b* expression using quantitative RT-PCR (Table 1). *Akr1a1b* was abundantly expressed throughout embryonic and larval stages (Figure 1A) and also in all analyzed adult organs with the highest expression being in livers (Figure 1B). As mouse *akr1a1* is highly expressed in the kidney tubular system (Zhou et al., 2019), we assessed Akr1a1b expression in adult zebrafish kidneys by immunohistochemical staining and demonstrated a similar localization in the tubular system as described in mice (Figure 1C). Last, gene sequence alignment of Akr1a1 across different species showed that zebrafish Akr1a1a shares a 60% amino acid similarity with human Akr1a1, and a 58.1% similarity with mouse Akr1a1. For zebrafish Akr1a1b the similarity is 70.5% with human Akr1a1 and 69.3% with mouse Akr1a1 (Figure S1).

To address the physiological role of *akr1a1b* in zebrafish development and physiology, we have established a permanent knockout model using CRISPR-Cas9 technology. Following the injection of the gRNA together with Cas9 RNA targeting exon 4 of the zebrafish *akr1a1b* gene (Figure S2A), two different frameshift mutants were identified and used for the subsequent studies, including a 17-bp insertion in the *Tg(wt1b:EGFP)* reporter line labeling the embryonic pronephros (Perner et al., 2007) and a 23-bp deletion in the *Tg(fli1:EGFP)* reporter line labeling endothelial cells (Lawson and Weinstein, 2002) (Figure 2A). *Akr1a1b*$^{-/-}$ larvae showed a strong decrease of total Akr enzyme activity (Figure 2C), and Akr1a1b protein expression in adult livers was utterly abolished (Figure 2B). Activities of other carbonyl-detoxifying enzymes as potential compensatory mechanism, including glyoxalase 1 (Glo1) and aldehyde dehydrogenase (ALDH) enzymes, were not altered (Figures S2B and S2C). Interestingly, concentration of the dicarbonyl methylglyoxal (MG) (Figure 2D), but not of 3-deoxyglucosone, and glyoxal (Figures S2D and S2E) as reactive metabolites leading to Advanced Glycation Endproducts (Brownlee, 2001), was significantly increased in 96-hpf *akr1a1b*$^{-/-}$ larvae. Together, the data have proved the successful generation and validation of *akr1a1b* mutant zebrafish, which only shows an increase for MG.

Akr1a1b Knockout in Zebrafish Caused Alterations of the Embryonic Pronephros and of Adult Kidneys

As Akr1a1b is prominently expressed in zebrafish renal tubules (Figure 1C), we hypothesized a significant effect for *akr1a1b* knockout on kidney development and kidney function in zebrafish. The zebrafish pronephros starts to develop at 16 hpf and reach their full functionality at 96 hpf. Structurally, at 48 hpf, the zebrafish pronephros are simply composed of two nephrons and functionally consist of two blood-filtering glomeruli, although leaky at this time; two proximal and distal tubules; and the pronephric duct (Drummond and Davidson, 2010). In the morphological analysis in *Tg(wt1b:EGFP)* line, compared with the *akr1a1b*$^{+/+}$ embryos at 48 hpf, *akr1a1b*$^{-/-}$ embryos displayed an enlarged glomerulus, where the length was substantially increased from 88.6 $\pm$ 10.8 μm in the *akr1a1b*$^{+/+}$ to 106.3 $\pm$ 19.1 μm in *akr1a1b*$^{-/-}$ mutants. The pronephric neck was significantly shortened to 74.9 $\pm$ 19.3 μm in *akr1a1b*$^{-/-}$ embryos compared with 97.9 $\pm$ 14.6 μm in the *akr1a1b*$^{+/+}$ group (Figures 3A and 3B).

Gene	Sequencing
akr1a1b	CGTCTCTATTAAAAACTCTGAAAGACC
	AAGGGGTATCGCCTCGTT
Cpepck	ATCACGCATCGCTAAAGAGG
	CCGCTGCGAAATACTTCTTC
gls b	GGATATGGAGCAGCGTGATT
	CTCATCCATTGGTGTGTTGC
glud 1a	CCGGTATAACCTTGGGCTGG
	CTCGGGTCTGCGTGGATAAG
glut 1a	TGACCGGCCCATACGTTTTC
	ATCATCTCGGTTATATTTATCTGCC
glut 2	GCAGAAGAACCCTCACTC
	TCTCCGCCACAATAAACC
sglt 1	TGGAACGCTCTGGTTGTTGT
	TAGATGCGGATTCGCTGACC
sglt 2	ATGAGTCGGGTGCTTTCTGG
	ATGGCGCAGGGTAAAGACAA
b2m	ACTGCTGAAGAACGGACAGG
	GCAACGCTCTTTGTGAGGTG
β-actin	ACGGTCAGGTCATCACCATC
	TGGATACCGCAAGATTCCAT

Table 1. Primers Used for RT-qPCR

Furthermore, to evaluate whether renal functionality was affected by the knockout of *akr1a1b*, we assessed the pronephric ultrafiltration in zebrafish larvae. Upon sinus venous injection of the 70-kDa Texas Red dextran, a significantly increased loss of fluorescence in *akr1a1b*$^{-/-}$ (the ratios are 0.516 $\pm$ 0.079 and 0.364 $\pm$ 0.079 at 24 and 48 hpf, respectively) compared with the *akr1a1b*$^{+/+}$ larvae (the ratios are 0.621 $\pm$ 0.090 and 0.427 $\pm$ 0.076 at 24 and 48 hpi, respectively) was observed (Figure 3C). Thus, the result indicated an altered glomerular filtration rate in the *akr1a1b* knockout zebrafish. Based on the findings in *akr1a1b*$^{-/-}$ embryos, we performed a histological and electron microscopy analysis of adult *akr1a1b*$^{-/-}$ kidneys to address whether the pronephros developmental impairments in embryos persisted into adult zebrafish (Figure 4). In most adult *akr1a1b*$^{-/-}$ kidneys, a deposition of diastase-resistant periodic acid-Schiff-positive hyaline droplets, putatively lysosomes, with a mild to a moderate amount and a small to medium size within the epithelium of proximal tubules was found (Figures 4A and 4B). In contrast, the kidneys of *akr1a1b*$^{+/+}$ animals only have scattered and mostly small droplets (Figures 4A and 4B), which were valued as a physiological finding as known from other animal species (Decker et al., 2012; Sato et al., 2005). As livers showed the highest *akr1a1b* expression (Figure 1B), we also analyzed the histology of adult *akr1a1b*$^{-/-}$ livers (Figure 4C). Yet, the overall morphology was not altered in this organ. Taken together, knockout of *akr1a1b* in zebrafish altered the embryonic pronephros and adult kidney, but other organs, including the liver, appeared normal.

Glutamate Accumulated in *akr1a1b* Knockout Zebrafish and Caused Pronephros Alterations

To investigate the underlying mechanisms of the pronephric and renal abnormalities, we performed metabolic profiling, including analysis of several amino acids, glycolytic and Krebs cycle intermediates, fatty acids, and adenosines in *akr1a1*$^{-/-}$ and *akr1a1b*$^{+/+}$ zebrafish larvae at 96 hpf. Most intermediates were

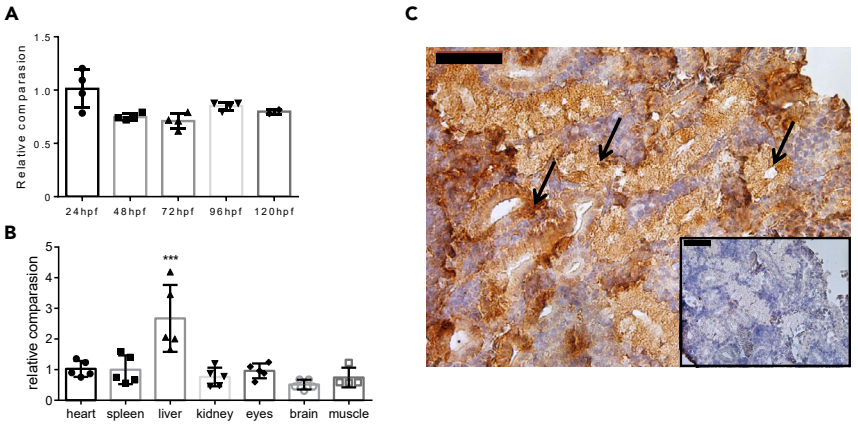

Figure 1. Expression of *akr1a1b* in Zebrafish Development and in Adult Organs

(A and B) (A) Akr1a1b is ubiquitously expressed in zebrafish development (relatively compared with 24 hpf, n = 4, mean ± SD) and (B) in all analyzed organs of adult zebrafish (relatively compared with heart, n = 5, mean ± SD).

(C) In adult zebrafish kidney, immunohistochemistry revealed high Akr1a1b expression in renal tubules (arrows). Box shows kidney immunostaining with secondary antibody only. Expression of genes in (A and B) was determined by RT-qPCR and normalized to β-actin.

***p < 0.001, p value was calculated by one-way ANOVA. Scale bars, 50 μm. See also Figure S1.

not significantly changed except for 2-keto glutaric acid and citric acid (Figure S3). Yet, interestingly, we found increased concentrations of two glucogenic amino acids, namely, glutamate and alanine (Figure 5A).

To test the hypothesis that elevated concentrations of glutamate and alanine may cause the observed pronephros phenotype in *akr1a1b*$^{-/-}$ mutants (Figure 3), *Tg(wt1b:EGFP)* embryos were incubated for 48 h in medium containing increasing concentrations of glutamate and alanine, and subsequently, the pronephros was analyzed. In zebrafish treated with 0.1 and 1 mM glutamate, the glomerular length was increased to 89.6 ± 10.9 μm and 91.8 ± 9.8 μm, respectively, whereas it was 82.6 ± 9.1 μm in egg water. The pronephric neck was shortened to 100.3 ± 14.5 μm and 88.8 ± 15.5 μm, respectively, whereas it was 111.3 ± 12.6 μm in egg water (Figures 5C and 5D). In addition, wild-type zebrafish larvae treated with 1 mM glutamate showed a significantly increased loss of fluorescence after 70-kDa Texas Red dextran injection (the ratios are 0.513 ± 0.084 and 0.350 ± 0.052 at 24 and 48 hpi, respectively), compared with larvae treated with egg water (the ratios are 0.620 ± 0.107 and 0.432 ± 0.052 at 24 and 48 hpi, respectively) (Figure 5E). In zebrafish treated with 5 mM alanine, the glomerular length was altered to 75.8 ± 8.5 μm and 87.1 ± 6.1 μm, respectively, whereas it was 77.6 ± 11.3 μm in control conditions. The pronephric neck was shortened to 127.2 ± 15.6 μm and 105.4 ± 9.3 μm, respectively, whereas it was 131.4 ± 22.0 μm in egg water (Figure S4). In conclusion, although both amino acids induced pronephric alterations, glutamate (0.1 mM) was more detrimental than alanine (5 mM). These results suggest glutamate as the main damaging factor of pronephric changes in *akr1a1b*$^{-/-}$ zebrafish embryos.

Next, we aimed to verify whether the accumulation of glutamate and alanine persisted into adult zebrafish. Therefore we measured concentrations of both amino acids in the kidneys and livers at 2, 3, and 18 h postprandial. Glutamate was significantly enriched in *akr1a1*$^{-/-}$ adult zebrafish kidneys at 3 h postprandial stage, to 2.90 ± 0.29 nmol/mg tissue, and at 18 h postprandial stage, to 6.63 ± 1.29 nmol/mg tissue; meanwhile, it was 1.96 ± 0.15 nmol/mg tissue and 3.14 ± 0.37 nmol/mg tissue in *akr1a1b*$^{+/+}$ zebrafish kidneys, respectively (Figure 5B). In contrast, the concentration of alanine was unchanged in kidneys as it was for glutamate and alanine in adult livers (Figure S5). Thus, increased concentrations of glutamate were only identified in *akr1a1b*$^{-/-}$ kidneys.

Altered Gluconeogenesis in *akr1a1b*$^{-/-}$ Zebrafish

Glutamate and alanine are glucogenic amino acids serving as primary substrates for gluconeogenesis in kidneys and livers, respectively. The accumulation of glutamate in *akr1a1b*$^{-/-}$ embryos and in adult *akr1a1b*$^{-/-}$ kidneys led to the hypothesis of dysfunctional gluconeogenesis, specifically in *akr1a1b*$^{-/-}$ kidneys. Glucose synthesis by gluconeogenesis in the human kidney accounts for approximately 20% of total glucose production in the body in the postabsorptive state (Gerich et al., 2001), and alterations of glucose synthesis may affect glucose homeostasis. To test if glucose homeostasis is altered in adult *akr1a1b*$^{-/-}$ mutants, we measured blood glucose

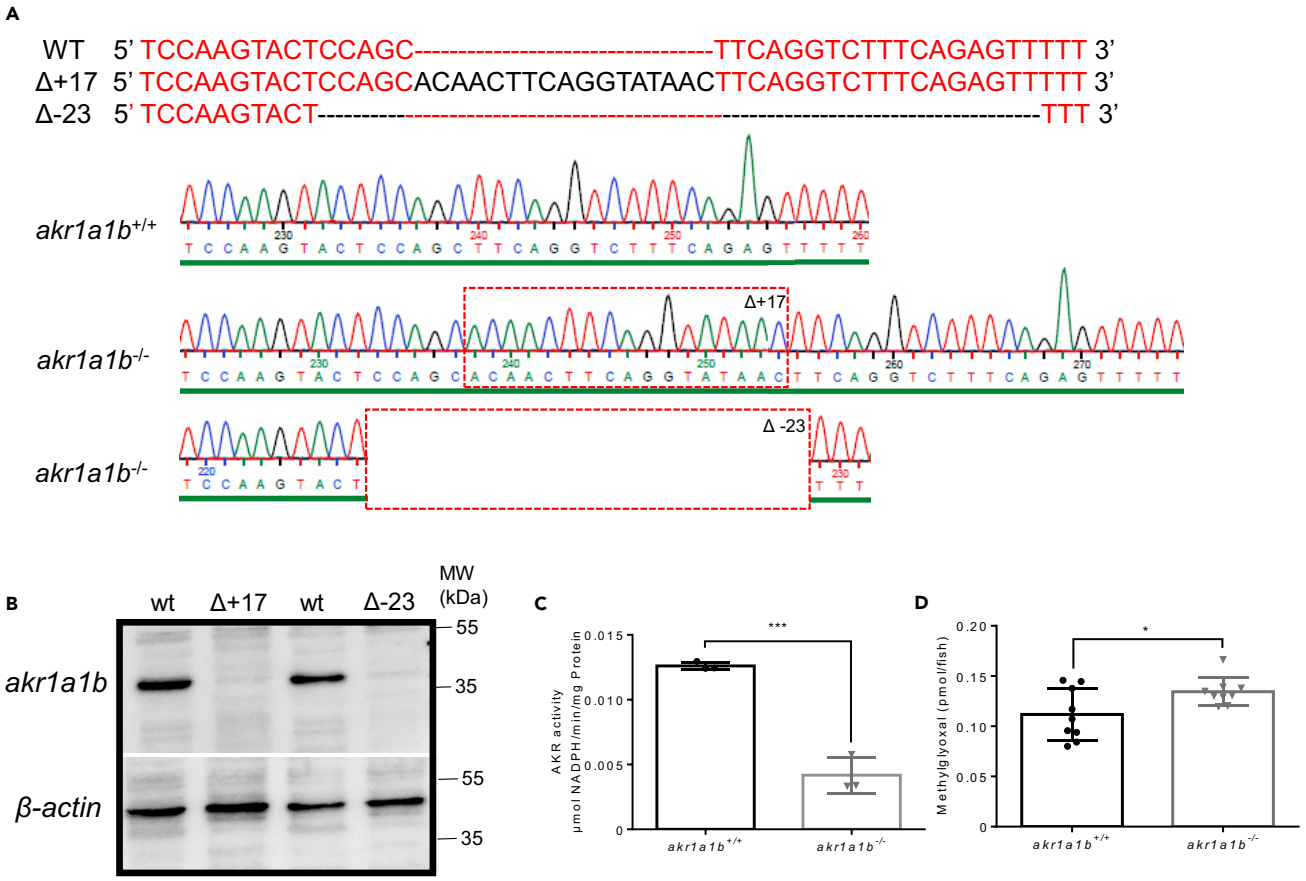

Figure 2. Generation and Validation of *akr1a1b*$^{-/-}$ Zebrafish Mutants

(A) CRISPR-Cas9 technology was used to establish *akr1a1b* knockout zebrafish. Schematic depiction of wild-type *akr1a1b* target sequence and two identified frameshift mutations and their corresponding chromatograms including a 17-bp insertion (Δ+17) in the *Tg(wt1b:EGFP)* reporter line and a 23-bp deletion (Δ-23) in the *Tg(fli1:EGFP)* reporter line. Red dashed boxes indicate start of genomic alterations.

(B) Western blot for Akr1a1b expression in zebrafish livers showed absence of Akr1a1b protein in the 17-bp insertion (Δ+17) and in the 23-bp deletion mutant (Δ-23), respectively, which validates the *akr1a1b* knockout zebrafish model. Beta-actin served as loading control.

(C) Δ+17 *akr1a1b*$^{-/-}$ zebrafish larvae at 96 hpf showed a strong descend of Akr enzyme activity (n = 3 clutches with 50 larvae, mean ± SD).

(D) Δ+17/Δ-23 *akr1a1b*$^{-/-}$ larvae at 96 hpf have increased MG concentrations (n = 9 clutches with 50 larvae).

*p < 0.05, ***p < 0.001, p value was calculated by t test. See also Figure S2.

concentrations of adult zebrafish at 2, 3, and 18 h postprandial and we found hypoglycemia after overnight fasting with blood glucose concentrations of 26.12 ± 5.50 mg/dL in *akr1a1b*$^{-/-}$ zebrafish significantly lower compared with 34.29 ± 15.66 mg/dL in *akr1a1b*$^{+/+}$ zebrafish (Figure 6A). Yet, blood glucose levels 2 h and 3 h after feeding were not changed in *akr1a1b*$^{-/-}$ zebrafish indicating physiological glucose metabolism after glucose uptake. Thus, the data suggest inhibition of gluconeogenesis in *akr1a1b*$^{-/-}$ mutants, especially in kidneys, because renal gluconeogenesis accounts for the major glucose production in the prolonged fasting stage.

Gluconeogenesis is regulated by different mechanisms. Among the genes involved in gluconeogenesis regulation, the critical rate-limiting enzyme is PEPCK (Figure 6B), whose activity is directly related by its mRNA abundance (Quinn and Yeagley, 2005). Thus, we compared PEPCK expression (Table 1) in livers and kidneys between *akr1a1b*$^{+/+}$ and *akr1a1b*$^{-/-}$ adult zebrafish after 2, 3, and 18 h postprandial. In addition, important genes (Table 1) involved in glutamate metabolism and glucose transportation, including *glutamate dehydrogenase 1 (glud 1), Glutaminase (gls), glut 1 (glucose transporter 1), glut 2 (glucose transporter 2), sglt 1 (sodium dependent glucose co-transporter 1),* and *sglt 2 (sodium dependent glucose co-transporter 2)*, in the kidney were also measured (Figure S6). It was found that PEPCK expression 2 h after feeding remained unaltered in *akr1a1b*$^{-/-}$ livers and kidneys, whereas 3 h and 18 h postprandial, PEPCK expression in *akr1a1b*$^{-/-}$ kidneys was significantly reduced (Figures 6C and 6D). Together, the data indicated that *akr1a1b* deficiency in zebrafish blocks PEPCK expression

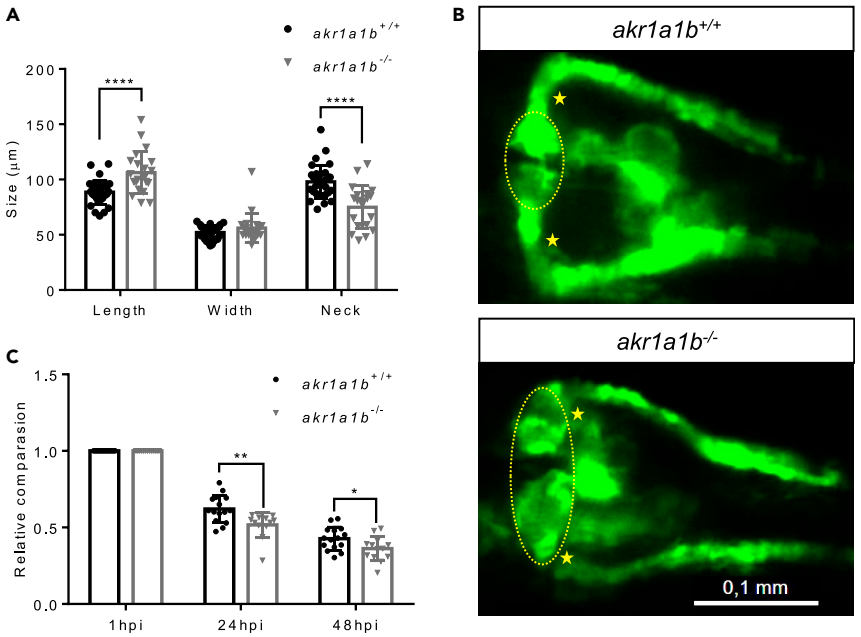

Figure 3. *Akr1a1b* Knockout in Zebrafish Caused Alterations of the Embryonic Pronephros

(A) Compared with *akr1a1b*$^{+/+}$ embryos (n = 33, mean ± SD) at 48 hpf, Δ+17 *akr1a1b*$^{-/-}$ mutants (n = 21, mean ± SD) displayed an enlarged glomerulus (encircled) and shortened tubular neck (asterisk). (B) Representative pronephros images of 48hpf old *akr1a1b*$^{+/+}$ and Δ+17 *akr1a1b*$^{-/-}$ embryos.

(C) A significant increased loss of fluorescence in Δ+17*akr1a1b*$^{-/-}$ mutants (n = 18, mean ± SD) was observed when compared with *akr1a1b*$^{+/+}$ larvae (n = 21, mean ± SD), which indicated an altered glomerular filtration rate in *akr1a1b*$^{-/-}$ mutants.

*p < 0.05, **p < 0.01, ****p < 0.0001, p value was calculated by t test. Scale bar: 0.1 mm.

in kidneys leading to inhibition of gluconeogenesis, accompanied by hypoglycemic episodes and renal glutamate accumulation promoting kidney alterations.

Akr1a1b Regulates S-Nitrosylation

A recent study in mice has proved that Akr1a1 mediates glucose metabolism by inhibiting S-nitrosylation of glycolytic enzymes (Zhou et al., 2019). Thus, we hypothesized an altered S-nitrosylation as the upstream mechanism regulating kidney malformation in *akr1a1b*$^{-/-}$ mutants. First, we determined nitrotyrosine as a marker for nitrosative stress in 96-hpf *akr1a1b*$^{-/-}$ larvae and found a strong increase (Figure 7A). Second, SNO (S-nitrosylated protein) levels were measured by western blot, revealing that SNOs were highly increased in kidneys of *akr1a1b*$^{-/-}$ zebrafish (Figure 7B). These data pointed to an increased stimulation of S-nitrosylation in *akr1a1b*$^{-/-}$ zebrafish.

To investigate whether evaluated S-nitrosylation may account for kidney alterations observed in *akr1a1b*$^{-/-}$ embryos, *akr1a1b*$^{+/+}$ and *akr1a1b*$^{-/-}$ embryos were treated with 20 μM L-NAME, a known inhibitor of nitric oxide formation (Figure S7). It was found that inhibition of S-nitrosylation by L-NAME treatment in *akr1a1b*$^{-/-}$ embryos normalized the alterations of the pronephros at 48 hpf (Figures 7C and 7D). In addition, we analyzed if PEPCK expression is regulated by S-nitrosylation and therefore determined PEPCK expression in 96-hpf *akr1a1b*$^{-/-}$ larvae after L-NAME treatment. PEPCK expression was increased in 96-hpf L-NAME-treated *akr1a1b*$^{+/+}$ larvae, whereas PEPCK expression in *akr1a1b*$^{-/-}$ larvae compared with *akr1a1b*$^{+/+}$ larvae was slightly decreased, but could be significantly increased and normalized to *akr1a1b*$^{+/+}$ levels after L-NAME treatment (Figure 7E). Altogether, the data have proved that altered gluconeogenesis and glutamate accumulation in *akr1a1b*$^{-/-}$ zebrafish caused by enriched SNOs accounted for the underlying kidney abnormalities.

DISCUSSION

In this study, we have established zebrafish Akr1a1b as a regulator of gluconeogenesis by regulating PEPCK expression and thereby maintaining glucose homeostasis. Loss of *akr1a1b* leads to hypoglycemia

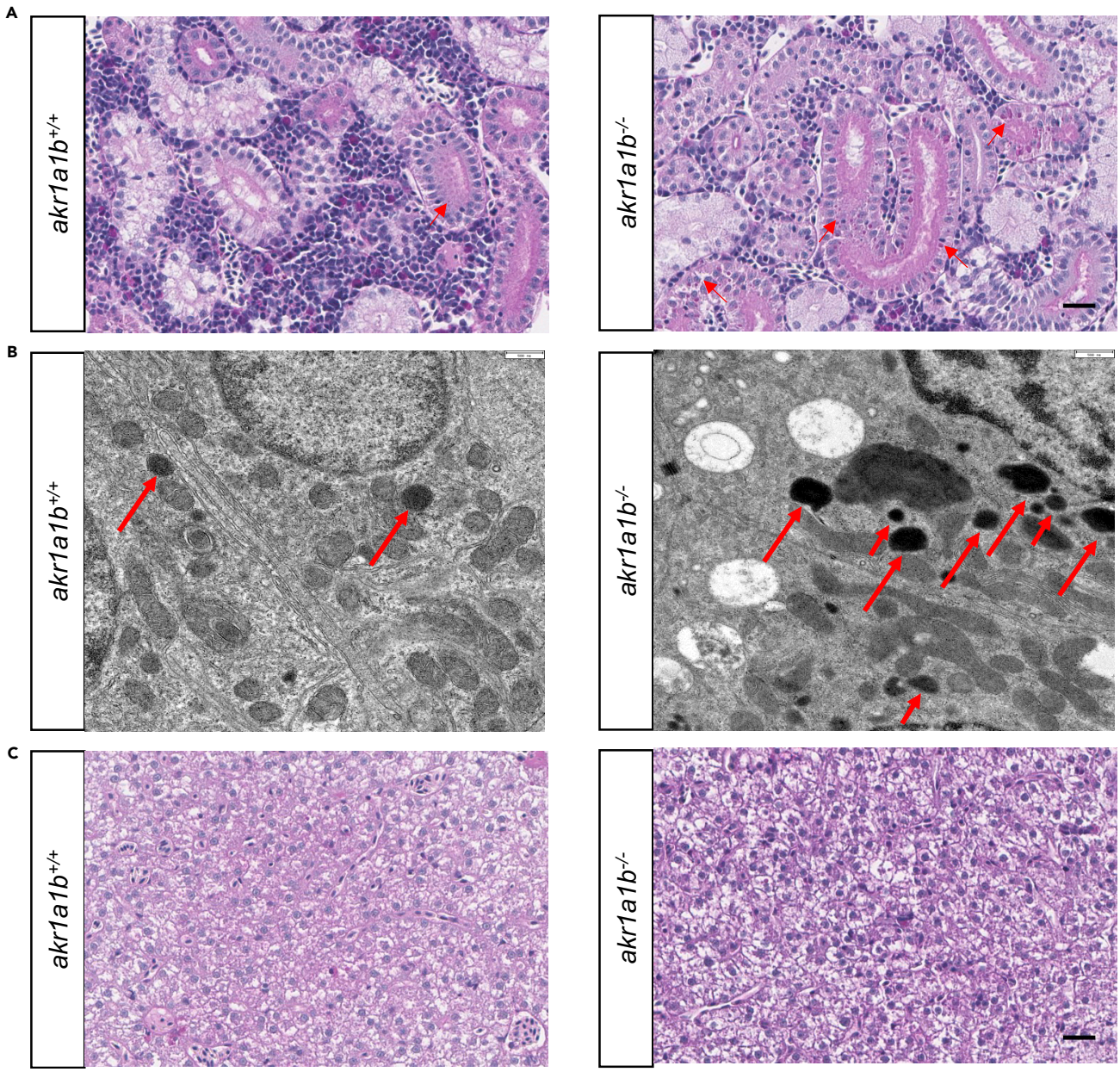

Figure 4. *Akr1a1b* Knockout Altered Adult Zebrafish Kidneys, but Livers Remained Normal

(A) Periodic acid-Schiff (PAS) staining and (B) electron microscopy (EM) showed deposition of diastase-resistant PAS-positive hyaline droplets, putatively lysosomes (red arrows), within the epithelium of proximal tubules in Δ-23 *akr1a1b*$^{-/-}$ kidneys. *Akr1a1b*$^{+/+}$ kidneys only have scattered small droplets. Quantification of 19 *akr1a1b*$^{-/-}$ EM images revealed 9 images with "+" and 10 images with "++" PAS-positive hyaline droplets. All 20 *akr1a1b*$^{+/+}$ EM images were scored as "0."

(C) Adult Δ-23 *akr1a1b*$^{-/-}$ livers stained by PAS were unaltered.

Scale bars: 20 μm in (A and C) and 500 nm (B).

and glutamate accumulation, which severely damages the pronephros, and this process is regulated by NO-dependent S-nitrosylation.

The most important finding of the study is the identification of a regulatory mechanism of how glucose homeostasis is controlled. Although glucose is an essential energy substrate for the body with, e.g., the human brain requiring 130 g glucose a day (Cunnane et al., 2011), continuously increased or decreased blood

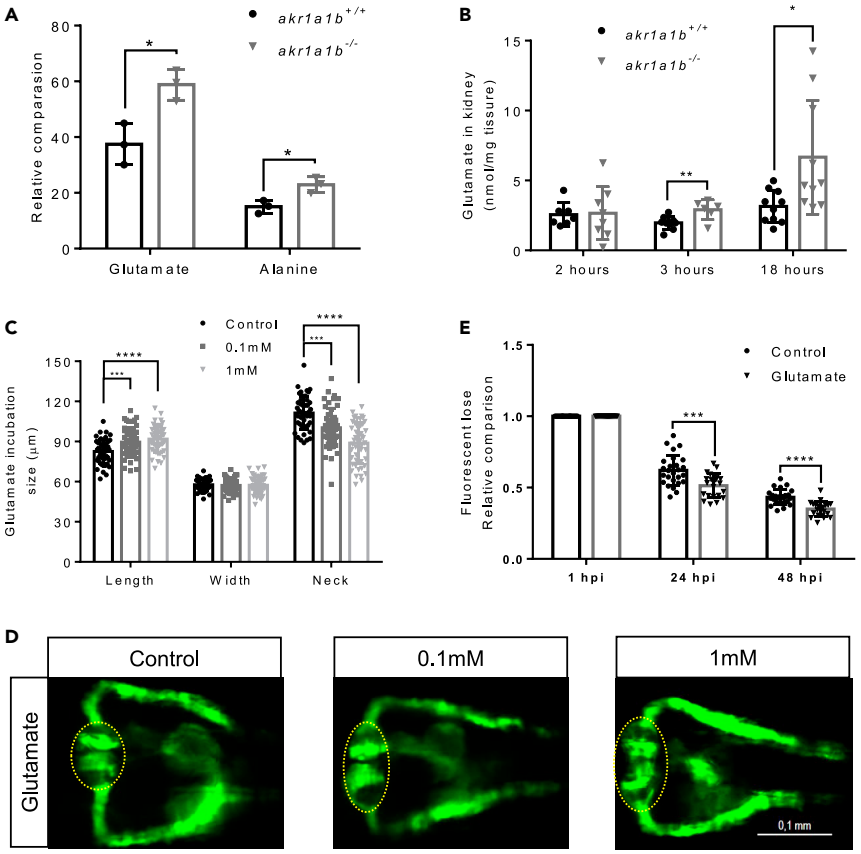

Figure 5. Glutamate Accumulation in *akr1a1b*$^{-/-}$ Mutants Damaged the Kidneys

(A) Primary metabolites were measured in 96-hpf larvae by gas chromatography-mass spectrometry analysis and showed a significant increase for glutamate and alanine in Δ+17 *akr1a1b*$^{-/-}$ larvae (n = 3 clutches with 50 larvae, mean ± SD).

(B) Glutamate accumulated in adult Δ+17/Δ-23 *akr1a1b*$^{-/-}$ zebrafish kidneys at 3 and 18 h postprandial (2 h postprandial: n = 7 in *akr1a1b*$^{+/+}$, n = 8 in *akr1a1b*$^{-/-}$; 3 h postprandial: n = 9 in *akr1a1b*$^{+/+}$, n = 6 in *akr1a1b*$^{-/-}$; 18 h postprandial: n = 10 in both groups, mean ± SD).

(C) Enlarged glomerulus and shortened tubular neck length in 48-hpf wild-type zebrafish embryos treated with glutamate (n = 46 in control group; n = 50 in 0.1 mM group; n = 49 in 1 mM group, mean ± SD). (D) Representative pronephros images of glutamate treated 48hpf embryos. Glomeruli are encircled.

(E) A significant increased loss of fluorescence in 1 mM glutamate-treated wild-type larvae both at 24 and 48 hpi (n = 26 in control group; n = 21 in 1 mM group, mean ± SD).

*p < 0.05, **p < 0.01, ***p < 0.001, ****p < 0.0001; p value in (A, B, and E) was calculated by t test, p value in (C) was calculated by one-way ANOVA, Scale bar, 0.1 mm. See also Figures S3, S4, and S5.

glucose levels lead to severe metabolic diseases. Diabetes, defined by hyperglycemia, is the most common metabolic disease leading to several organ alterations (Roglic and World Health Organization, 2016), and glucose-induced metabolic changes have been identified as one crucial damaging mechanism (Borg et al., 2011; Diabetes et al., 1993; Duckworth et al., 2009; UKPDS, 1998). In contrast, severe hypoglycemia is also a life-threatening condition, accompanied by heart racing, nausea, trembling, and sweating (Tesfaye and Seaquist, 2010) and can lead to greater risk of cardiovascular events (Zinman et al., 2018), seizure (Buckingham et al., 2008), coma, and death (Zoungas et al., 2010). Hypoglycemic conditions are typically seen in diabetic patients induced by inappropriate insulin usage but may also be caused by other metabolic conditions. These observations strongly suggest that maintaining physiological glucose homeostasis is a fundamental process and highlights zebrafish Akr1a1b as a regulator of this process. The function of the Akr gene family has mostly been mysterious, and only a few genes have functionally been analyzed in more detail thus far. Akr1b1 has attracted most attention in the past because it can convert glucose to sorbitol, has an increased activity during diabetes, and inhibition of Akr1b1 has been suggested as a promising approach to prevent diabetic complications (Brownlee, 2001). Yet, although preclinical studies were promising, later clinical trials failed (Singh et al., 2015). A recent study in mice highlighted a function

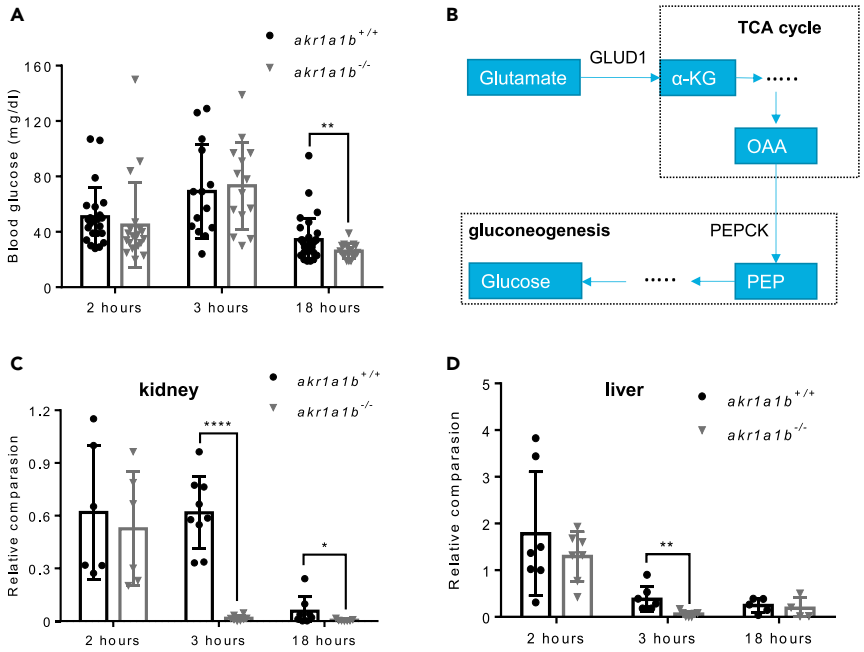

Figure 6. Inhibition of Gluconeogenesis Led to Hypoglycemia in Overnight Fasted *akr1a1b*$^{-/-}$ Zebrafish

(A) Blood glucose was measured at different time points after feeding in adult *akr1a1b*$^{+/+}$ and Δ+17/Δ-23 *akr1a1b*$^{-/-}$ zebrafish and found hypoglycemia after overnight fasting in *akr1a1b*$^{-/-}$ zebrafish (2 h postprandial: n = 23 in *akr1a1b*$^{+/+}$, n = 20 in *akr1a1b*$^{-/-}$; 3 h postprandial: n = 14 in *akr1a1b*$^{+/+}$, n = 14 in *akr1a1b*$^{-/-}$; 18 h postprandial: n = 31 in *akr1a1b*$^{+/+}$, n = 16 in *akr1a1b*$^{-/-}$, mean ± SD).

(B) Schematic depiction of gluconeogenesis and how glucogenic amino acid glutamate serves as substrate. PEPCK: phosphoenolpyruvate carboxykinase; PEP: phosphoenolpyruvate; OAA: oxaloacetate; α-KG: α-ketoglutarate; GLUD1: glutamate dehydrogenase 1.

(C) Loss of cytosolic cPEPCK expression in adult Δ+17/Δ-23 *akr1a1b*$^{-/-}$ kidneys 3 and 18 h after feeding (2 h postprandial: n = 6 in *akr1a1b*$^{+/+}$, n = 6 in *akr1a1b*$^{-/-}$; 3 h postprandial: n = 9 in *akr1a1b*$^{+/+}$, n = 8 in *akr1a1b*$^{-/-}$; 18 h postprandial: n = 8 in *akr1a1b*$^{+/+}$, n = 7 in *akr1a1b*$^{-/-}$, mean ± SD).

(D) Loss of cytosolic cPEPCK expression in adult Δ+17/Δ-23 *akr1a1b*$^{-/-}$ livers 3 h after feeding (2 h postprandial: n = 7 in *akr1a1b*$^{+/+}$, n = 7 in *akr1a1b*$^{-/-}$; 3 h postprandial: n = 7 in *akr1a1b*$^{+/+}$, n = 7 in *akr1a1b*$^{-/-}$; 18 h postprandial: n = 5 in *akr1a1b*$^{+/+}$, n = 4 in *akr1a1b*$^{-/-}$, mean ± SD). cPEPCK expression was analyzed by RT-qPCR and normalized to *b2m*. *p < 0.05, **p < 0.01, ****p < 0.0001, p value was calculated by t test. See also Figure S6.

for another Akr family member, namely, Akr1a1. It was shown that Akr1a1 has an S-nitroso-CoA reductase activity, and *akr1a1* knockout mice were protected from acute kidney injury (Zhou et al., 2019).

Interestingly, Akr1a1 has been suggested as a regulator of glucose homeostasis in mice by regulating S-nitrosylation of pyruvate kinase 2 (PKM2) and thereby affecting its activity. In detail, S-nitrosylation of PKM2 blocked its activity and subsequently pyruvate production (Zhou et al., 2019). In contrast to mice and humans, the zebrafish genome contains only a few *akr* family members, but for *akr1a1*, two genes, namely, *akr1a1a* and *akr1a1b* are present in the zebrafish genome. In this study, Akr1a1b was identified as a regulator of gluconeogenesis, which regulates NO-dependent S-nitrosylation. Thus, although mouse Akr1a1 and zebrafish Akr1a1b both regulate glucose homeostasis, they act on reciprocal pathways, namely, glycolysis by Akr1a1 and gluconeogenesis by Akr1a1b. This leads now to the major question, if the other zebrafish *akr1a1* gene, namely, *akr1a1a*, is the functional homolog to mouse and human *akr1a1* and which gene in mouse and human is the functional counterpart to zebrafish *akr1a1b*? The opposite regulation of glucose homeostasis by mouse Akr1a1 regulating glycolysis and zebrafish Akr1a1b regulating gluconeogenesis suggests the concept that in both species opposite regulators exist and these unknown regulators must now be identified in future experimental studies.

The second important observation of the study is the identification of zebrafish Akr1a1b as a regulator S-nitrosylation and subsequently controlling PEPCK expression as the key regulatory enzyme in gluconeogenesis and that the inhibition of gluconeogenesis not only leads to hypoglycemic conditions but also

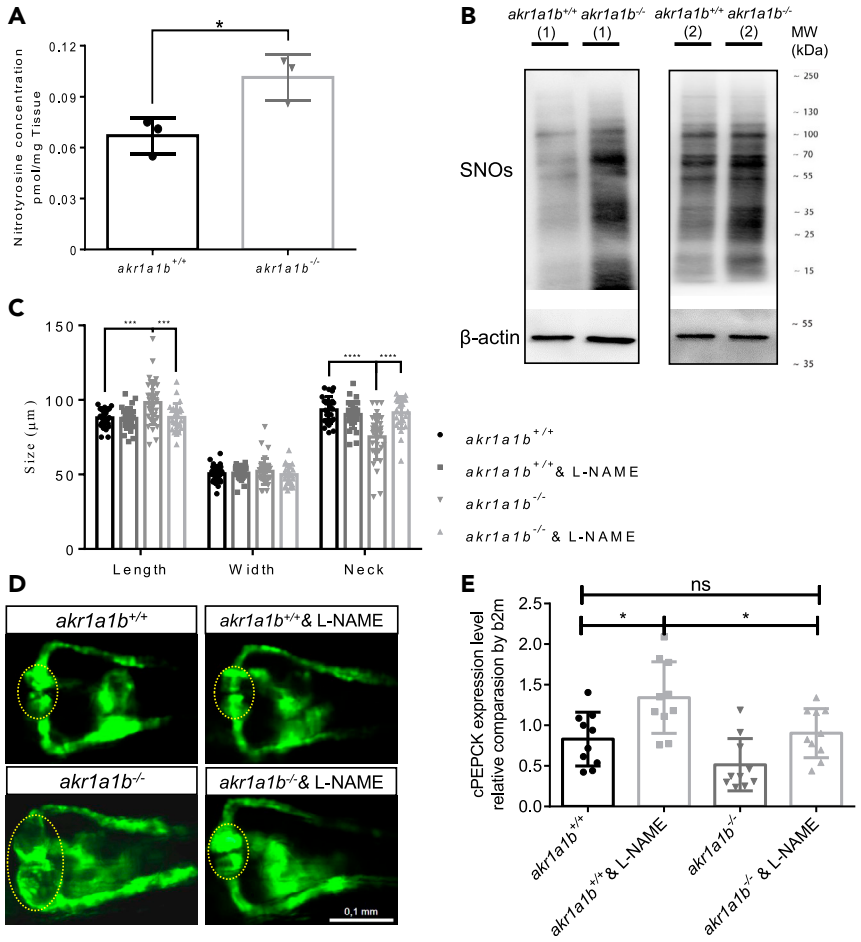

Figure 7. NO-Dependent S-Nitrosylation Regulated Gluconeogenesis and Pronephros Development in *akr1a1b*$^{-/-}$ Mutants

(A) Nitrotyrosine was measured by ultrahigh-performance liquid chromatography-mass spectrometry, and was increased in 96-hpf Δ-23 *akr1a1b*$^{-/-}$ larvae (n = 3 clutches with 50 larvae, mean ± SD).

(B) Western blots show increased S-nitrosylated proteins (SNOs) in adult Δ-23 *akr1a1b*$^{-/-}$ kidneys (n = 2).

(C) Inhibition of NO-dependent S-nitrosylation by L-NAME in Δ+17 *akr1a1b*$^{-/-}$ zebrafish 48-hpf embryos rescued the altered pronephros (n = 27 in *akr1a1b*$^{+/+}$ group; n = 27 in *akr1a1b*$^{+/+}$ & L-NAME group; n = 34 in *akr1a1b*$^{-/-}$ group; n = 25 in *akr1a1b*$^{-/-}$ & L-NAME group, mean ± SD).

(D) Representative pronephros images of 48hpf *akr1a1b*$^{+/+}$ and Δ+17 *akr1a1b*$^{-/-}$ embryos treated with L-NAME. Glomeruli are encircled.

(E) cPEPCK expression was regulated by S-nitrosylation. Inhibition of S-nitrosylation by L-NAME treatment increased cPEPCK expression in *akr1a1b*$^{+/+}$ and Δ-23 *akr1a1b*$^{-/-}$ encircled larvae at 96 hpf and normalized cPEPCK expression in *akr1a1b*$^{-/-}$ encircled larvae as measured by RT-qPCR (n = 10 in all groups, mean ± SD).

*p < 0.05, ***p < 0.001, ****p < 0.0001, p value in (A) was calculated by t test, p values of (C and E) were calculated by one-way ANOVA. Scale bar, 0.1 mm. See also Figure S7.

leads to glutamate accumulation in embryos and adult *akr1a1b*$^{-/-}$ kidneys and alters the embryonic pronephros and adult kidney. The data now have three important implications. First, it suggests the Akr family as a therapeutic target to block gluconeogenesis as it would be beneficial to prevent hyperglycemic conditions in diabetes. Alternatively, activation of the Akr enzymes could prevent severe hypoglycemia thereby preventing coma and death. Second, it shows that altered regulations of evolutionarily conserved pathways, such as gluconeogenesis, can lead to severe organ damage in the body. In *akr1a1b*$^{-/-}$ kidneys, we found an accumulation of glutamate, and we have proved in zebrafish embryos that glutamate treatment damaged the pronephros. Thus, prolonged altered concentrations of physiological metabolites, such as the amino acid glutamate, damage organs. Last, the data in *akr1a1b*$^{-/-}$ zebrafish have further

proved the different substrate preference for gluconeogenesis occurring in liver and kidney. Although in *akr1a1b*$^{-/-}$ embryos, both glucogenic amino acids alanine and glutamate, accumulated and damaged the embryonic pronephros, glutamate accumulation as the substrate for gluconeogenesis only occurred in adult kidneys. In contrast, alanine as the preferred substrate for gluconeogenesis in the liver remained normal.

In summary, the data have identified a mechanism of how glucose homeostasis is controlled. The Akr gene family and specifically the *akr1a1* genes have a major function in maintaining physiological blood glucose concentrations in different species and thereby controlling the important equilibrium between providing glucose-derived energy and preventing glucose-induced organ damage.

Limitations of the Study

In our study, we have generated *akr1a1b* mutant zebrafish, and we demonstrate that Akr1a1b regulates glucose homeostasis by controlling gluconeogenesis. Yet, the function of the gene homolog of *akr1a1b* in zebrafish, named *akr1a1a*, has so far been unknown, and it remains elusive what potential role it may have in glucose metabolism regulation. Furthermore, as zebrafish Akr1a1b has overlapping, but also different mechanisms when compared with mouse Akr1A1 in glucose metabolisms, and the mouse/human genome consists of several other *akr* genes, it has so far been unknown which mouse/human gene is the homolog to zebrafish Akr1a1b. Last, it must be further analyzed in detail how exactly Akr1a1b regulates cPEPCK expression.

Resource Availability

Lead Contact

Further information and requests for resources and reagents should be directed to and will be fulfilled by the Lead Contact: Jens Kroll (jens.kroll@medma.uni-heidelberg.de).

Materials Availability

The anti-Akr1a1b antibody and both *akr1a1b* zebrafish mutants generated in this study are available from the Lead Contact with a completed Materials Transfer Agreement.

Data and Code Availability

The published article includes all datasets generated or analyzed during this study. For Akr1a1b amino acid sequence, please refer to: https://www.uniprot.org/.

METHODS

All methods can be found in the accompanying Transparent Methods supplemental file.

SUPPLEMENTAL INFORMATION

Supplemental Information can be found online at https://doi.org/10.1016/j.isci.2020.101763.

ACKNOWLEDGMENTS

The study was supported by grants from Deutsche Forschungsgemeinschaft (CRC 1118 and IRTG 1874/2 DIAMICOM) and China Scholarship Council (CSC). The authors thank the Metabolomics Core Technology Platform of the Excellence cluster "CellNetworks" (Heidelberg University), the Deutsche Forschungsgemeinschaft (grant ZUK 40/2010-3009262) for support with ultra-performance liquid chromatography-based metabolite quantification, Prof. Dr. Ilse Hofmann & Claudia Tessmer from the CF Unit Antibodies from DKFZ Heidelberg, and Dr. Stefan Hillmer, Electron Microscopy Core Facility of Heidelberg University. The authors also acknowledge the support of the Zebrafish Core Facility of Medical Faculty Mannheim.

AUTHOR CONTRIBUTIONS

X.L. performed experiments, analyzed data, and wrote the manuscript. F.S., H.Q., K.B., C.T.T., G.P., N.V., T.P., I.H., J.M., and T.F. performed experiments and analyzed data. R.H. and P.P.N. gave conceptual advice. J.K. conceived and designed the study and wrote the manuscript. J.K. is the guarantor of this work and, as such, had full access to all the data in the study and takes responsibility for the integrity of the data and the accuracy of the data analysis.

DECLARATION OF INTERESTS

The authors report no conflict of interest.

Received: June 12, 2020
Revised: October 8, 2020
Accepted: October 30, 2020
Published: December 18, 2020

REFERENCES

Alsahli, M., and Gerich, J.E. (2017). Renal glucose metabolism in normal physiological conditions and in diabetes. Diabetes Res. Clin. Pract. *133*, 1–9.

Benoy, M.P., and Elliott, K.A.C. (1937). The metabolism of lactic and pyruvic acids in normal and tumour tissues V. Synthesis of carbohydrate. Biochem. J. *31*, 1268–1275.

Bergman, H., and Drury, D.R. (1938). The relationship of kidney function to the glucose utilization of the extra abdominal tissues. Am. J. Phys. *124*, 279–284.

Bjorkman, O., Felig, P., and Wahren, J. (1979). Gluconeogenesis by the human-kidney - unique stimulatory effect of fructose. Clin. Res. *27*, A409.

Bjorkman, O., Felig, P., and Wahren, J. (1980). The contrasting responses of splanchnic and renal glucose output to gluconeogenic substrates and to hypoglucagonemia in 60-H-fasted humans. Diabetes *29*, 610–616.

Borg, R., Kuenen, J.C., Carstensen, B., Zheng, H., Nathan, D.M., Heine, R.J., Nerup, J., Borch-Johnsen, K., Witte, D.R., and Grp, A.S. (2011). HbA(1c) and mean blood glucose show stronger associations with cardiovascular disease risk factors than do postprandial glycaemia or glucose variability in persons with diabetes: the A1C-Derived Average Glucose (ADAG) study. Diabetologia *54*, 69–72.

Brownlee, M. (2001). Biochemistry and molecular cell biology of diabetic complications. Nature *414*, 813–820.

Buckingham, B., Wilson, D.M., Lecher, T., Hanas, R., Kaiserman, K., and Cameron, F. (2008). Duration of nocturnal hypoglycemia before seizures. Diabetes Care *31*, 2110–2112.

Cunnane, S., Nugent, S., Roy, M., Courchesne-Loyer, A., Croteau, E., Tremblay, S., Castellano, A., Pifferi, F., Bocti, C., Paquet, N., et al. (2011). Brain fuel metabolism, aging, and Alzheimer's disease. Nutrition *27*, 3–20.

Decker, J.H., Dochterman, L.W., Niquette, A.L., and Brej, M. (2012). Association of renal tubular hyaline droplets with lymphoma in CD-1 mice. Toxicol. Pathol. *40*, 651–655.

Diabetes, C., Complications Trial Research, G., Nathan, D.M., Genuth, S., Lachin, J., Cleary, P., Crofford, O., Davis, M., Rand, L., and Siebert, C. (1993). The effect of intensive treatment of diabetes on the development and progression of long-term complications in insulin-dependent diabetes mellitus. N. Engl. J. Med. *329*, 977–986.

Drummond, I.A., and Davidson, A.J. (2010). Zebrafish kidney development. Method Cell Biol. *100*, 233–260.

Drury, D.R., Wick, A.N., and Mackay, E.M. (1950). Formation of glucose by the kidney. Am. J. Phys. *163*, 655–661.

Duckworth, W., Abraira, C., Moritz, T., Reda, D., Emanuele, N., Reaven, P.D., Zieve, F.J., Marks, J., Davis, S.N., Hayward, R., et al. (2009). Glucose control and vascular complications in veterans with type 2 diabetes. N. Engl. J. Med. *360*, 129–139.

Fagerberg, L., Hallstrom, B.M., Oksvold, P., Kampf, C., Djureinovic, D., Odeberg, J., Habuka, M., Tahmasebpoor, S., Danielsson, A., Edlund, K., et al. (2014). Analysis of the human tissue-specific expression by genome-wide integration of transcriptomics and antibody-based proteomics. Mol. Cell Proteomics *13*, 397–406.

Gerich, J.E., Meyer, C., Woerle, H.J., and Stumvoll, M. (2001). Renal gluconeogenesis - its importance in human glucose homeostasis. Diabetes Care *24*, 382–391.

Heckler, K., and Kroll, J. (2017). Zebrafish as a model for the study of microvascular complications of diabetes and their mechanisms. Int. J. Mol. Sci. *18*, 2002.

Jorgens, K., Stoll, S.J., Pohl, J., Fleming, T.H., Sticht, C., Nawroth, P.P., Hammes, H.P., and Kroll, J. (2015). High tissue glucose alters intersomitic blood vessels in zebrafish via methylglyoxal targeting the VEGF receptor signaling cascade. Diabetes *64*, 213–225.

Lawson, N.D., and Weinstein, B.M. (2002). In vivo imaging of embryonic vascular development using transgenic zebrafish. Dev. Biol. *248*, 307–318.

Lodd, E., Wiggenhauser, L.M., Morgenstern, J., Fleming, T.H., Poschet, G., Buttner, M., Tabler, C.T., Wohlfart, D.P., Nawroth, P.P., and Kroll, J. (2019). The combination of loss of glyoxalase1 and obesity results in hyperglycemia. JCI Insight *4*, e126154.

Lou, B., Boger, M., Bennewitz, K., Sticht, C., Kopf, S., Morgenstern, J., Fleming, T., Hell, R., Yuan, Z., Nawroth, P.P., et al. (2020). Elevated 4-hydroxynonenal induces hyperglycaemia via Aldh3a1 loss in zebrafish and associates with diabetes progression in humans. Redox Biol. *37*, 101723.

Meyer, C., Dostou, J.M., Welle, S.L., and Gerich, J.E. (2002). Role of human liver, kidney, and skeletal muscle in postprandial glucose homeostasis. Am. J. Physiol. endocrinol. Metab. *282*, E419–E427.

Meyer, C., Stumvoll, M., Nadkarni, V., Dostou, J., Mitrakou, A., and Gerich, J. (1998). Abnormal renal and hepatic glucose metabolism in type 2 diabetes mellitus. J. Clin. Invest. *102*, 619–624.

Olsen, A.S., Sarras, M.P., and Intine, R.V. (2010). Limb regeneration is impaired in an adult zebrafish model of diabetes mellitus. Wound Repair Regen. *18*, 532–542.

Perner, B., Englert, C., and Bollig, F. (2007). The Wilms tumor genes wt1a and wt1b control different steps during formation of the zebrafish pronephros. Dev. Biol. *309*, 87–96.

Petersen, M.C., Vatner, D.F., and Shulman, G.I. (2017). Regulation of hepatic glucose metabolism in health and disease. Nat. Rev. Endocrinol. *13*, 572–587.

Quinn, P.G., and Yeagley, D. (2005). Insulin regulation of PEPCK gene expression: a model for rapid and reversible modulation. Curr. Drug Targets Immune Endocr. Metabol. Disord. *5*, 423–437.

Roglic, G., and World Health Organization. (2016). Global Report on Diabetes (World Health Organization).

Sato, S., Kitamura, H., Ghazizadeh, M., Adachi, A., Sasaki, Y., Ishizaki, M., Inoue, K., Wakamatsu, K., and Sugisaki, Y. (2005). Occurrence of hyaline droplets in renal biopsy specimens: an ultrastructural study. Med. Mol. Morphol. *38*, 63–71.

Schmohl, F., Peters, V., Schmitt, C.P., Poschet, G., Buttner, M., Li, X., Weigand, T., Poth, T., Volk, N., Morgenstern, J., et al. (2019). CNDP1 knockout in zebrafish alters the amino acid metabolism, restrains weight gain, but does not protect from diabetic complications. Cell. Mol. Life Sci. *76*, 4551–4568.

Scotcher, D., Jones, C., Posada, M., Rostami-Hodjegan, A., and Galetin, A. (2016). Key to opening kidney for in vitro-in vivo extrapolation entrance in health and disease: Part I: in vitro systems and physiological data. AAPS J. *18*, 1067–1081.

She, J., Yuan, Z., Wu, Y., Chen, J., and Kroll, J. (2018). Targeting erythropoietin protects against proteinuria in type 2 diabetic patients and in zebrafish. Mol. Metab. *8*, 189–202.

Singh, M., Kapoor, A., and Bhatnagar, A. (2015). Oxidative and reductive metabolism of lipid-peroxidation derived carbonyls. Chem. Biol. Interact. *234*, 261–273.

Stumvoll, M., Perriello, G., Meyer, C., and Gerich, J. (1999). Role of glutamine in human

carbohydrate metabolism in kidney and other tissues. Kidney Int. *55*, 778–792.

Tesfaye, N., and Seaquist, E.R. (2010). Neuroendocrine responses to hypoglycemia. Ann. N. Y. Acad. Sci. *1212*, 12–28.

UKPDS (1998). Intensive blood-glucose control with sulphonylureas or insulin compared with conventional treatment and risk of complications in patients with type 2 diabetes (UKPDS 33). UK Prospective Diabetes Study (UKPDS) Group. Lancet *352*, 837–853.

Wiggenhauser, L.M., Qi, H., Stoll, S.J., Metzger, L., Bennewitz, K., Poschet, G., Krenning, G., Hillebrands, J.L., Hammes, H.P., and Kroll, J. (2020). Activation of retinal angiogenesis in hyperglycemic pdx1 (−/−) zebrafish mutants. Diabetes *69*, 1020–1031.

Yip, J., Geng, X., Shen, J., and Ding, Y. (2016). Cerebral gluconeogenesis and diseases. Front. Pharmacol. *7*, 521.

Yue, F., Cheng, Y., Breschi, A., Vierstra, J., Wu, W., Ryba, T., Sandstrom, R., Ma, Z., Davis, C., Pope, B.D., et al. (2014). A comparative encyclopedia of DNA elements in the mouse genome. Nature *515*, 355–364.

Zhou, H.L., Zhang, R., Anand, P., Stomberski, C.T., Qian, Z., Hausladen, A., Wang, L., Rhee, E.P., Parikh, S.M., Karumanchi, S.A., et al. (2019). Metabolic reprogramming by the S-nitroso-CoA reductase system protects against kidney injury. Nature *565*, 96–100.

Zinman, B., Marso, S.P., Christiansen, E., Calanna, S., Rasmussen, S., and Buse, J.B.; LEADER Publication Committee on behalf of the LEADER Trial Investigators (2018). Hypoglycemia, cardiovascular outcomes, and death: the LEADER experience. Diabetes Care *41*, 1783–1791.

Zoungas, S., Patel, A., Chalmers, J., de Galan, B.E., Li, Q., Billot, L., Woodward, M., Ninomiya, T., Neal, B., MacMahon, S., et al. (2010). Severe hypoglycemia and risks of vascular events and death. N. Engl. J. Med. *363*, 1410–1418.

iScience, Volume *23*

Supplemental Information

Regulation of Gluconeogenesis by Aldo-keto-reductase 1a1b in Zebrafish

Xiaogang Li, Felix Schmöhl, Haozhe Qi, Katrin Bennewitz, Christoph T. Tabler, Gernot Poschet, Rüdiger Hell, Nadine Volk, Tanja Poth, Ingrid Hausser, Jakob Morgenstern, Thomas Fleming, Peter Paul Nawroth, and Jens Kroll

A

```
P14550 AK1A1_HUMAN          1   MAASCVLLHTGQKMPLIGLGTWKSEPGQVKAAVKYALSVGYRHIDCAAIYGNEPEIGEAL      60
Q9JII6 AK1A1_MOUSE          1   MTASSVLLHTGQKMPLIGLGTWKSEPGQVKAAIKHALSAGYRHIDCASVYGNETEIGEAL      60
Q6AZW2 A1A1A_DANRE          1   -MTATITLSTGQRMPTVGLGTWKSAPGQVKQAVLAALDCGYRHIDCAAAYSNEREVGEAL      59
                                  :: : * ***:** :******* ***** *:  **. ********: *.** *:****

P14550 AK1A1_HUMAN         61   KEDVGPGKAVPREELFVTSKLWNTKHHPEDVEPALRKTLADLQLEYLDLYLMHWPYAFER     120
Q9JII6 AK1A1_MOUSE         61   KESVGSGKAVPREELFVTSKLWNTKHHPEDVEPALRKTLADLQLEYLDLYLMHWPYAFER     120
Q6AZW2 A1A1A_DANRE         60   TERLGPGKSLRRDDIFVTSKLWNTKHHPDDVEEACRRSLSDLRLSYLDLYLIHWPMAFGR     119
                                .* :* **:: *:::**************:*** * *::*:**:*.******:*** ** *

P14550 AK1A1_HUMAN        121   GDNPFPKNADGTICYDSTHYKETWKALEALVAKGLVQALGLSNFNSRQIDDILSVASVRP     180
Q9JII6 AK1A1_MOUSE        121   GDNPFPKNADGTVRYDSTHYKETWKALEVLVAKGLVKALGLSNFNSRQIDDVLSVASVRP     180
Q6AZW2 A1A1A_DANRE        120   GDELIPRHPDGTIQYDDTHYRDIWAAMEKLVDQGLAKAIGLSNFNAKQIDDILSIAKHKP     179
                                **: :*:: ***: **.***:** *:* ** :**.:*:******::****:**:*. :*

P14550 AK1A1_HUMAN        181   AVLQVECHPYLAQNELIAHCQARGLEVTAYSPLGSSDRAWRDPDEPVLLEEPVVLALAEK     240
Q9JII6 AK1A1_MOUSE        181   AVLQVECHPYLAQNELIAHCHARGLEVTAYSPLGSSDRAWRHPDEPVLLEEPVVLALAEK     240
Q6AZW2 A1A1A_DANRE        180   VVNQVECHPYLVQAELVSHCWSRNLTVTAYSPLGSPDRPWVTPGEALLLDDPRVVGIAKS     239
                                .* ********.* **:** :*.* ********* ** *  *.* :**:** *:.:*:.

P14550 AK1A1_HUMAN        241   YGRSPAQILLRWQVQRKVICIPKSITPSRILQNIKVFDFTFSPEEMKQLNALNKNWRYIV     300
Q9JII6 AK1A1_MOUSE        241   HGRSPAQILLRWQVQRKVICIPKSINPSRILQNIQVFDFTFSPEEMKQLDALNKNWRYIV     300
Q6AZW2 A1A1A_DANRE        240   YNKTPAQVIIRWHIQRGVVCIPKSVTPSRIKQNIEVFDFKLSDEDMRLIESFNRNERFII     299
                                :.::***:::**::** *:*****:.**** ***:****.:* *:*: ::::*:* *:*:

P14550 AK1A1_HUMAN        301   PMLTVDGKRVPRDAGHPLYPFNDPY                                 325
Q9JII6 AK1A1_MOUSE        301   PMITVDGKRVPRDAGHPLYPFNDPY                                 325
Q6AZW2 A1A1A_DANRE        300   PTVIKDGQKIWRDAKHPHFPFIEPY                                 324
                                * :  **::: *** ** :** :**
```

B

```
P14550      AK1A1_HUMAN       1   -MAASCVLLHTGQKMPLIGLGTWKSEPGQVKAAVKYALSVGYRHIDCAAIYGNEPEIGEA      59
Q9JII6      AK1A1_MOUSE       1   -MTASSVLLHTGQKMPLIGLGTWKSEPGQVKAAIKHALSAGYRHIDCASVYGNETEIGEA      59
A0A2R8QTH3 A0A2R8QTH3_DANRE   1   MSMNDFAVLSTGRKMPLLGLGTWKSEPGLVKQAVIWALESGYRHIDCAPIYANEPEIGEA      60
                                      . .:* **:****:********** ** *:  **. ******** :*.** *****

P14550      AK1A1_HUMAN      60   LKEDVGPGKAVPREELFVTSKLWNTKHHPEDVEPALRKTLADLQLEYLDLYLMHWPYAFE     119
Q9JII6      AK1A1_MOUSE      60   LKESVGSGKAVPREELFVTSKLWNTKHHPEDVEPALRKTLADLQLEYLDLYLMHWPYAFE     119
A0A2R8QTH3 A0A2R8QTH3_DANRE 61   FQETMGPDKGIRREDVFVTSKLWNTKHHPDDVEPSLLKTLKDLKLEYLDLYLIHWPYAFQ     120
                                 ::* :* .*.: **::**************:****:* *** **:********:******:

P14550      AK1A1_HUMAN      120   RGDNPFPKNADGTICYDSTHYKETWKALEALVAKGLVQALGLSNFNSRQIDDILSVASVR     179
Q9JII6      AK1A1_MOUSE      120   RGDNPFPKNADGTVRYDSTHYKETWKALEVLVAKGLVKALGLSNFNSRQIDDVLSVASVR     179
A0A2R8QTH3 A0A2R8QTH3_DANRE121   RGDTPFPRKEDGTLLYDDIDYKLIWAAMEKLVGKGLVRAIGLSNFNSRQIDDILSVASIK     180
                                 ***.***:: ***: **. .** ** *:* **.****:*:************:*****::

P14550      AK1A1_HUMAN      180   PAVLQVECHPYLAQNELIAHCQARGLEVTAYSPLGSSDRAWRDPDEPVLLEEPVVLALAE     239
Q9JII6      AK1A1_MOUSE      180   PAVLQVECHPYLAQNELIAHCHARGLEVTAYSPLGSSDRAWRHPDEPVLLEEPVVLALAE     239
A0A2R8QTH3 A0A2R8QTH3_DANRE181   PIVLQVESHPYLAQVELLSHCRDRGLVMTAYSPLGSPDRAWKHPDEPVLLEEPAIAALAK     240
                                 *:******.****** **::**: *** :********* ****:.**********.: ***:

P14550      AK1A1_HUMAN      240   KYGRSPAQILLRWQVQRKVICIPKSITPSRILQNIKVFDFTFSPEEMKQLNALNKNWRYI     299
Q9JII6      AK1A1_MOUSE      240   KHGRSPAQILLRWQVQRKVICIPKSINPSRILQNIQVFDFTFSPEEMKQLDALNKNWRYI     299
A0A2R8QTH3 A0A2R8QTH3_DANRE241   KYNKTPAQIIIRWQTQRGVVTIPKSITQSRIKENIQVFDFTLESEEMSQVTALHRGWRYI     300
                                 *:.::*****::***.** *: ******. *** :**:******:. ***.*: **::.****

P14550      AK1A1_HUMAN      300   VPMLTVDGKRVPRDAGHPLYPFNDPY                                325
Q9JII6      AK1A1_MOUSE      300   VPMITVDGKRVPRDAGHPLYPFNDPY                                325
A0A2R8QTH3 A0A2R8QTH3_DANRE301   VPTITVDGKSVPRDAGHPHYPFNDPY                                326
                                 ** :****** ******** *******
```

Supplement Figure 1: Sequence alignment of Akr1a1 across different species, related to Figure 1

Amino acid alignment shows a high similarity between the different species of the active site (red frame); first line: human Akr1a1; second line: mouse Akr1a1; third line:**(a)** zebrafish Akr1a1a, **(b)** zebrafish Akr1a1b (AOA2R8QTH3).

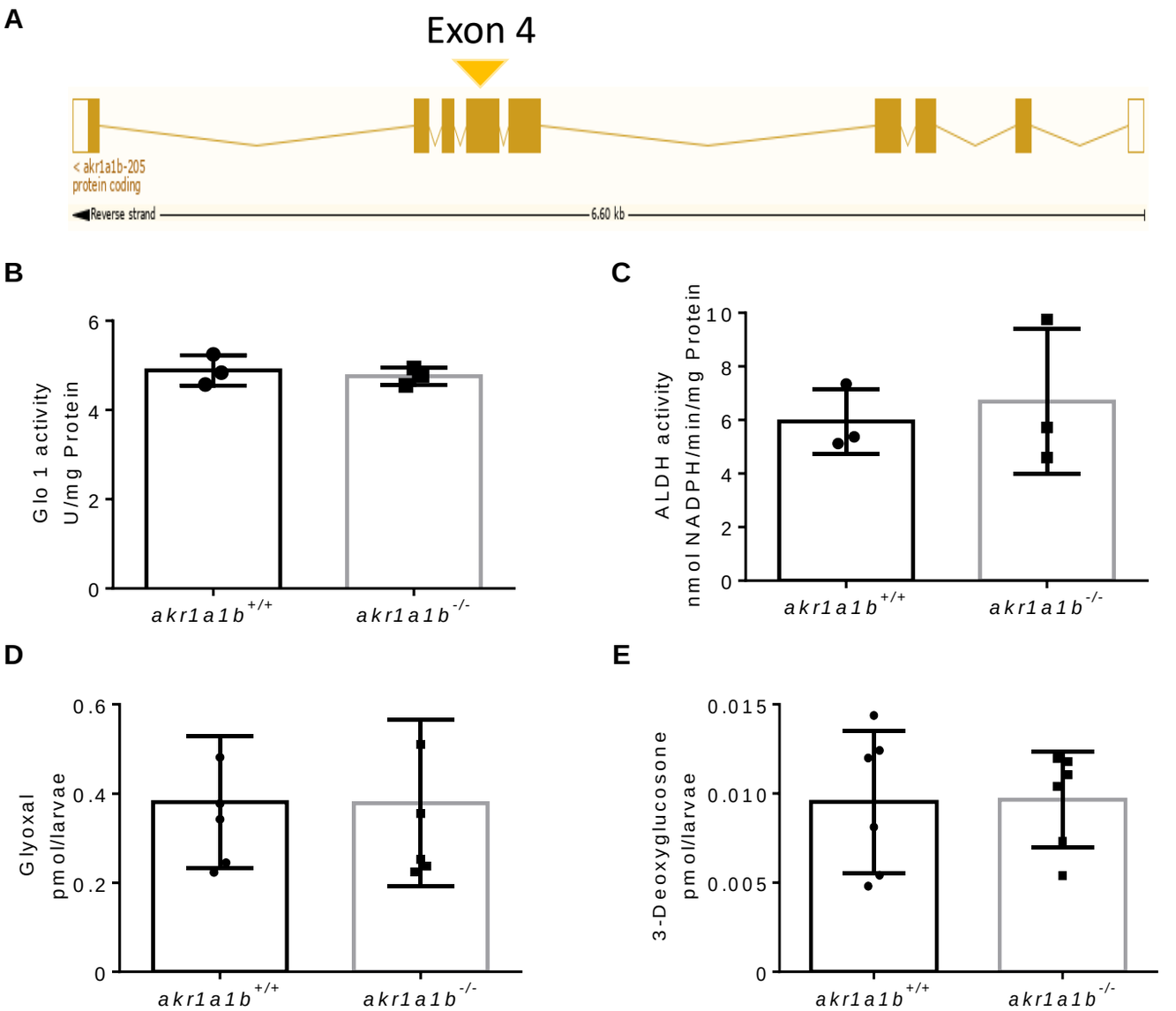

Supplement Figure 2: Characterization of *akr1a1b*$^{-/-}$ zebrafish, related to Figure 2
(a) Schematic depiction of the *akr1a1b* gene, which highlights exon 4 as CRISPR-Cas9 target site(https://www.ensembl.org/Danio_rerio/Transcript/Summary?db=core;g=ENSDARG00000052030;r=6:33918813-33925432;t=ENSDART00000145019). **(b,c)** Activity of compensatory enzymes, Glyoxalase 1 (Glo1) and Aldehyde Dehydrogenases (ALDH), were not altered as measured by spectrophotometric analysis in Δ-23 *akr1a1b*$^{-/-}$ zebrafish lysates at 96 hpf (n = 3 clutches with 50 larvae, mean ± SD). **(d,e)** Advanced Glycation End Products (AGEs) precursors Glyoxal and 3-Deoxyglucosone, were not altered in Δ-23 *akr1a1b*$^{-/-}$ 96 hpf old larvae, as determined by LC-MS/MS (D, E. n = 6 clutches with 50 larvae).

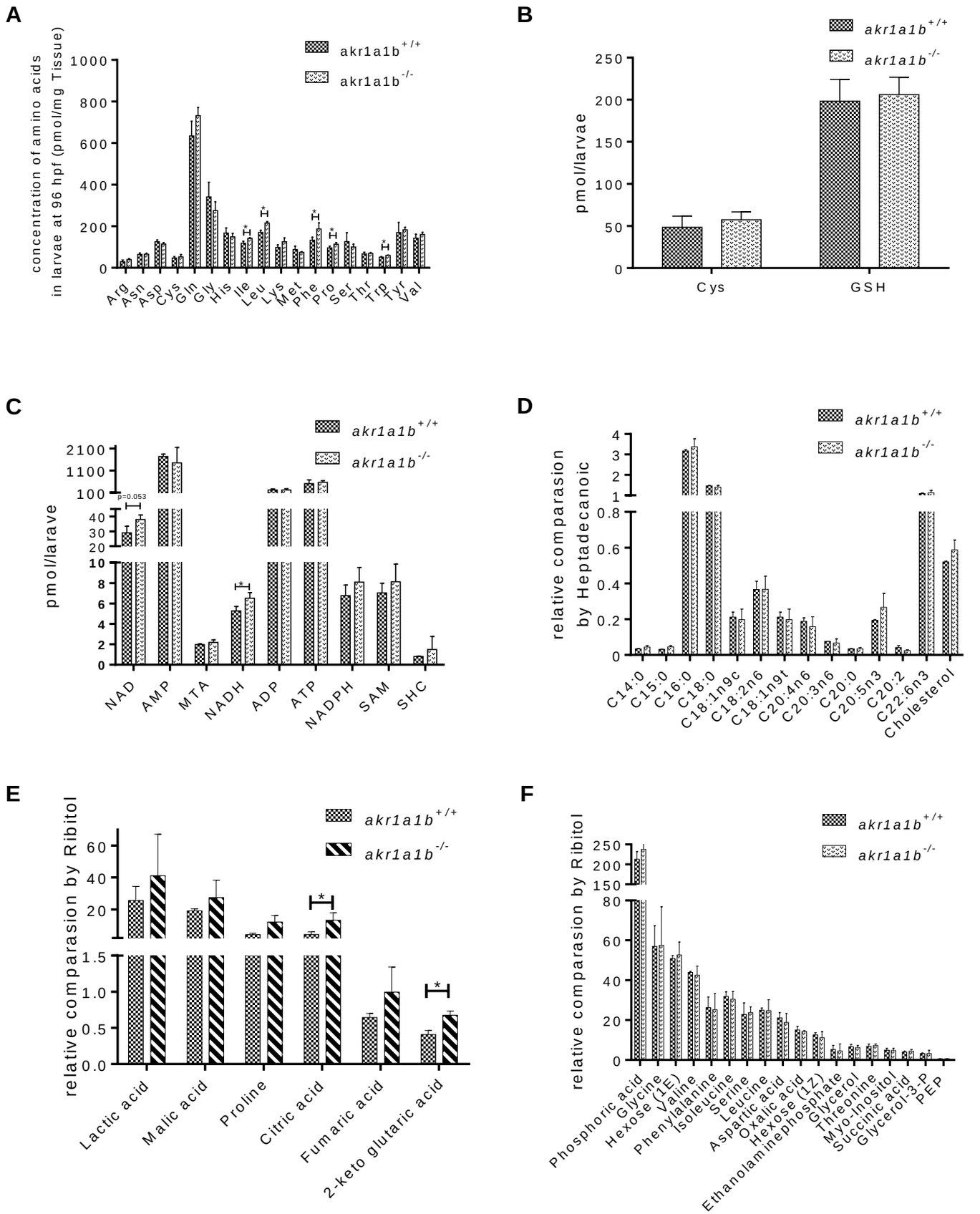

Supplement Figure 3: Metabolome profile in Δ-23 ***akr1a1b*$^{-/-}$ larvae, related to Figure 5**

(a) Amino acids, **(b)** thiols and **(c)** adenosine were slightly or not changed in *akr1a1b*$^{-/-}$ larvae as determined by using UPLC-FLR in zebrafish lysates at 96 hpf (n = 3 clutches with 50 larvae; mean ± SD). **(d)** Fatty acid and **(e,f)** primary metabolites were determined using GC/MS and only 2- keto glutaric acid and citric acid were increased in *akr1a1b*$^{-/-}$ larvae at 96hpf (n = 3 clutches with 50 larvae; mean ± SD). *p<0.05.

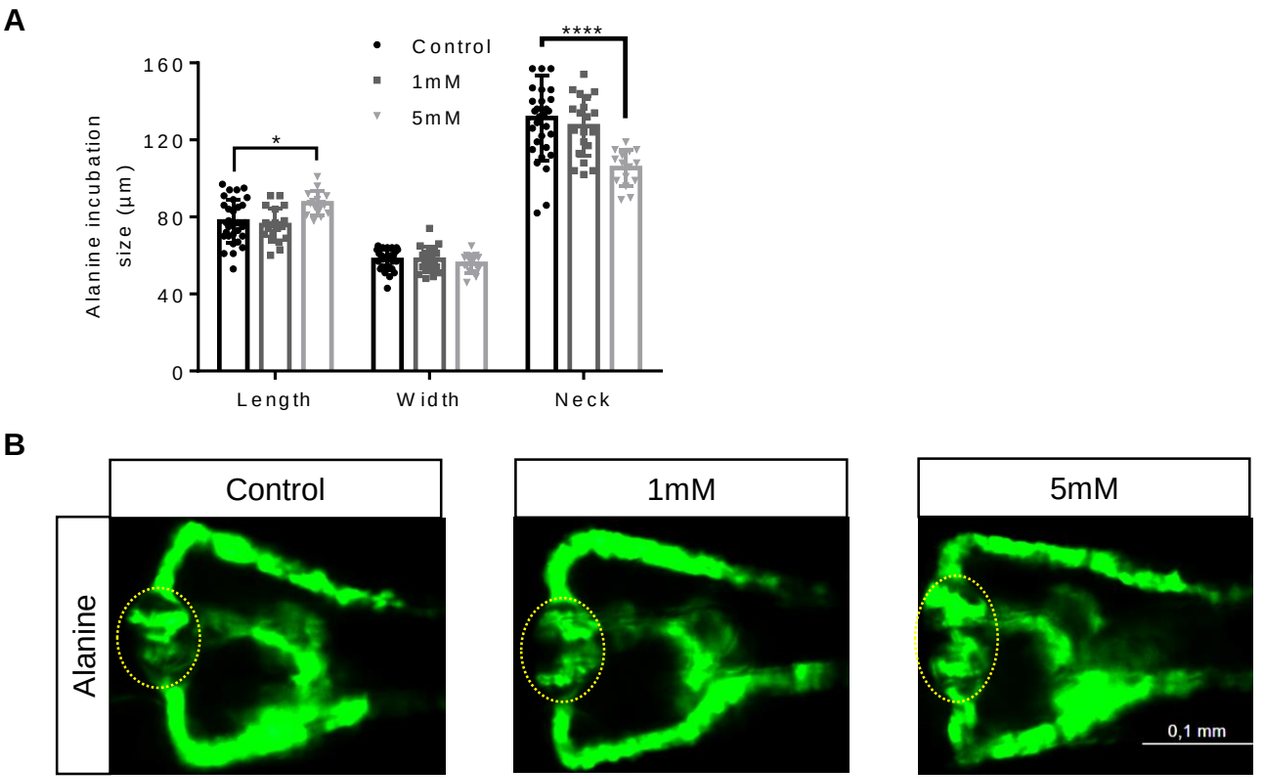

Supplement Figure 4: Alanine incubation of wild type embryos damaged the pronephros, related to Figure 5

(a,b) Enlarged glomerulus (encircled) and shortened tubular neck length in 48 hpf zebrafish embryos treated with alanine (n = 31 in control group; n = 20 in 0.1mM group; n = 15 in 1mM group , mean ± SD). * $p < 0.05$, **** $p < 0.0001$. Scale bar: 0.1 mm.

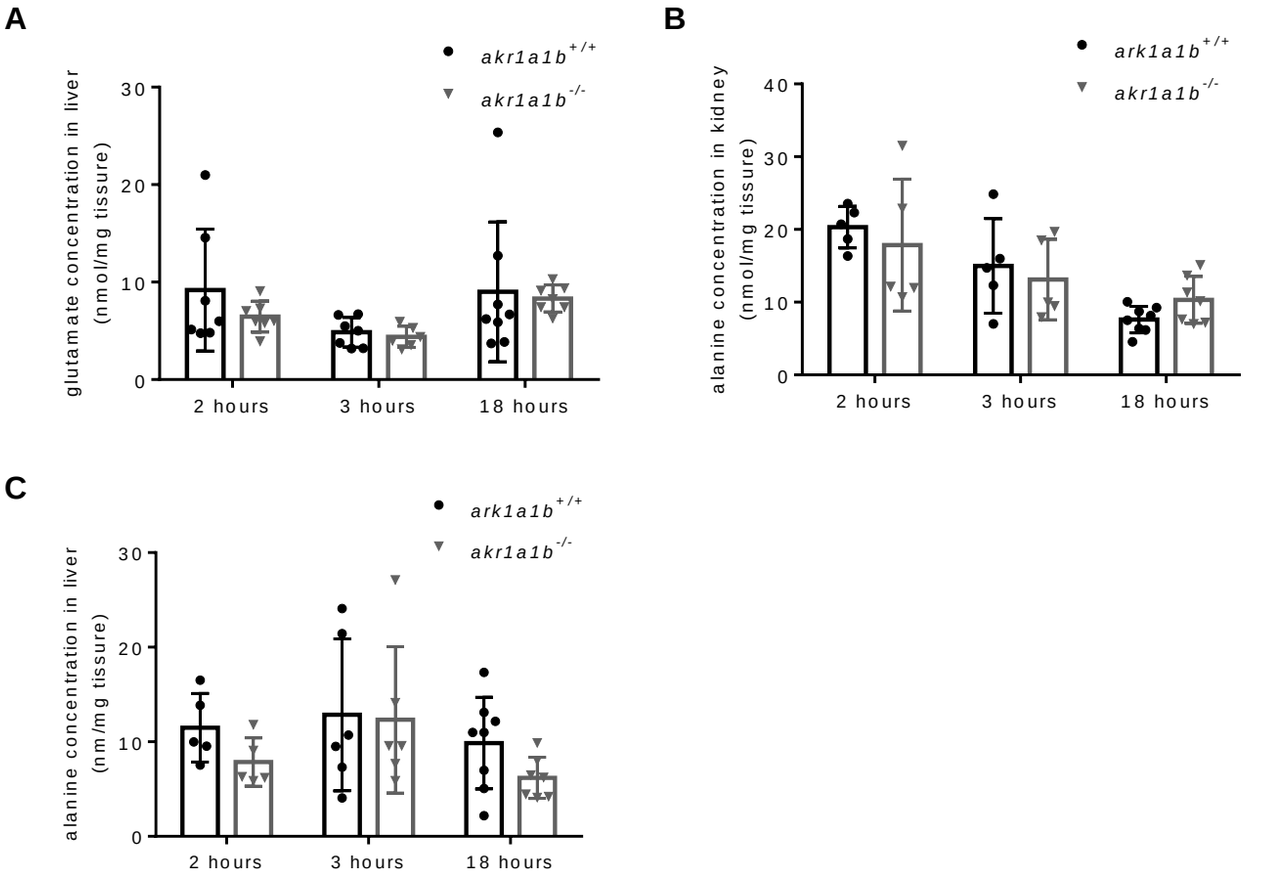

Supplement Figure 5: Unaltered concentrations of glutamate in Δ-23 *akr1a1b*$^{-/-}$ livers, and unaltered concentrations of alanine in Δ-23 *akr1a1b*$^{-/-}$ kidneys and livers, related to Figure 5

(a) Unaltered concentrations of glutamate in adult *akr1a1b*$^{-/-}$ livers (2 hours postprandial: n = 7 in *akr1a1b*$^{+/+}$, n = 7 in *akr1a1b*$^{-/-}$; 3 hours postprandial: n = 7 in *akr1a1b*$^{+/+}$, n = 6 in *akr1a1b*$^{-/-}$; 18 hours postprandial: n = 8 in *akr1a1b*$^{+/+}$, n = 7 in *akr1a1b*$^{-/-}$, mean ± SD). **(b,c)** Concentrations of alanine were not altered in adult *akr1a1b*$^{-/-}$ kidneys (2 hours postprandial: n = 5 in *akr1a1b*$^{+/+}$, n = 5 in *akr1a1b*$^{-/-}$; 3 hours postprandial: n = 5 in *akr1a1b*$^{+/+}$, n = 5 in *akr1a1b*$^{-/-}$; 18 hours postprandial: n = 8 in *akr1a1b*$^{+/+}$, n = 7 in *akr1a1b*$^{-/-}$,mean ± SD) and in adult *akr1a1b*$^{-/-}$ livers (2 hours postprandial: n = 5 in *akr1a1b*$^{+/+}$, n = 5 in *akr1a1b*$^{-/-}$; 3 hours postprandial: n = 5 in *akr1a1b*$^{+/+}$, n = 6 in *akr1a1b*$^{-/-}$; 18 hours postprandial: n = 8 in *akr1a1b*$^{+/+}$, n = 7 in *akr1a1b*$^{-/-}$, mean ± SD).

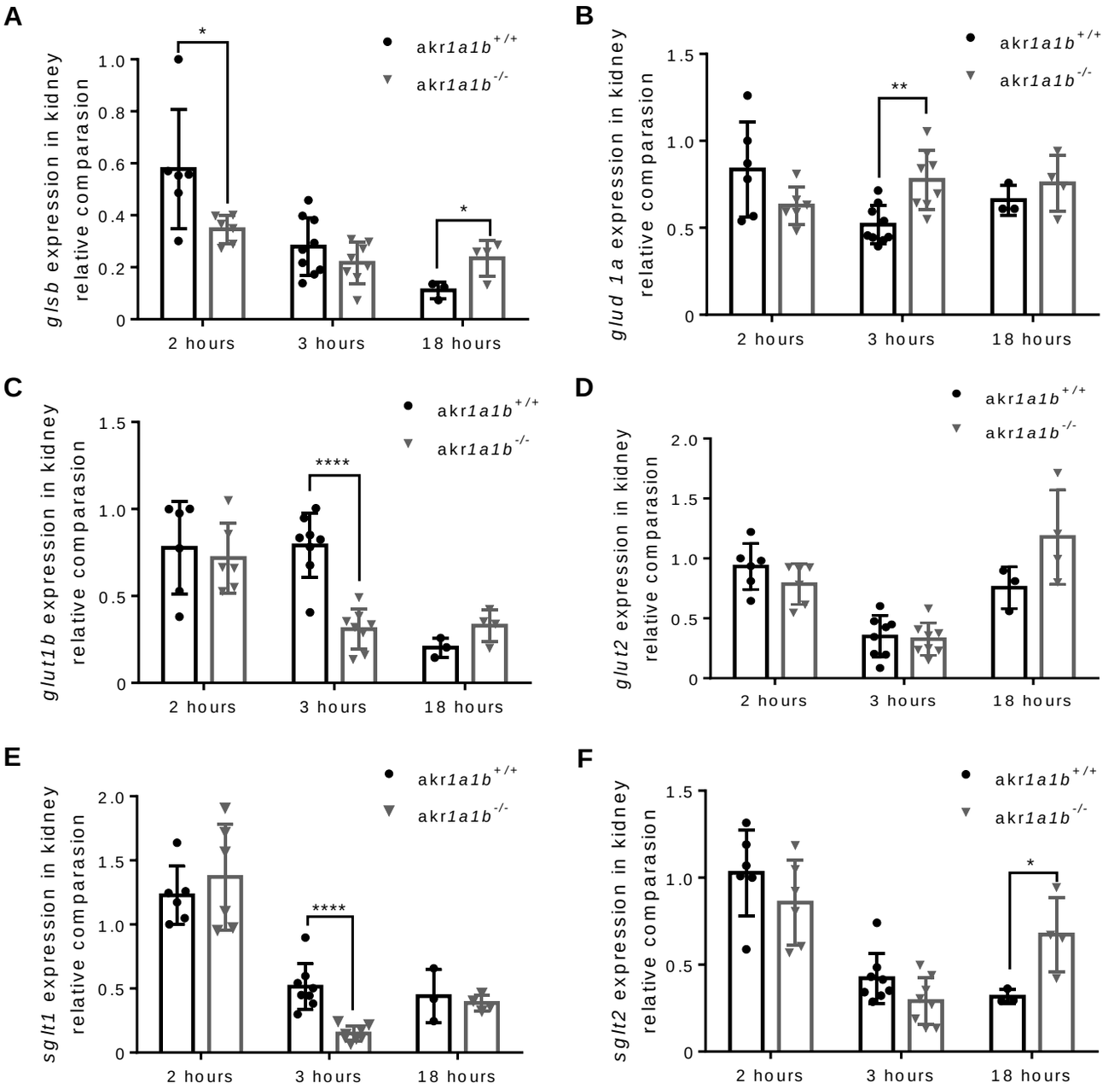

Supplement Figure 6: Expression of glutaminolytic enzymes and glucose transporters in Δ-23 *akr1a1b*$^{-/-}$ kidneys, related to Figure 6

Expression analysis of **(a)** *glutaminase* b (*glsb*), **(b)** *glutamate dehydrogenase 1 (glud1a)*, **(c)** *glucose transporter 1b* (*glut 1b)*, **(d)** glucose transporter 2 (*glut 2)*, **(e)** *sodium dependent glucose co-transporter 1 (sglt 1)* and **(f)** *sodium dependent glucose co-transporter 2 (sglt 2)* in adult *akr1a1b*$^{-/-}$ kidneys by RT-qPCR *(*2 hours postprandial: n = 6 in *akr1a1b*$^{+/+}$, n = 6 in *akr1a1b*$^{-/-}$; 3 hours postprandial: n = 9 in *akr1a1b*$^{+/+}$, n = 8 in *akr1a1b*$^{-/-}$; 18 hours postprandial: n = 3 in *akr1a1b*$^{+/+}$, n = 4 in *akr1a1b*$^{-/-}$, mean ± SD. * $p < 0.05$, ** $p < 0.01$, **** $p < 0.0001$.

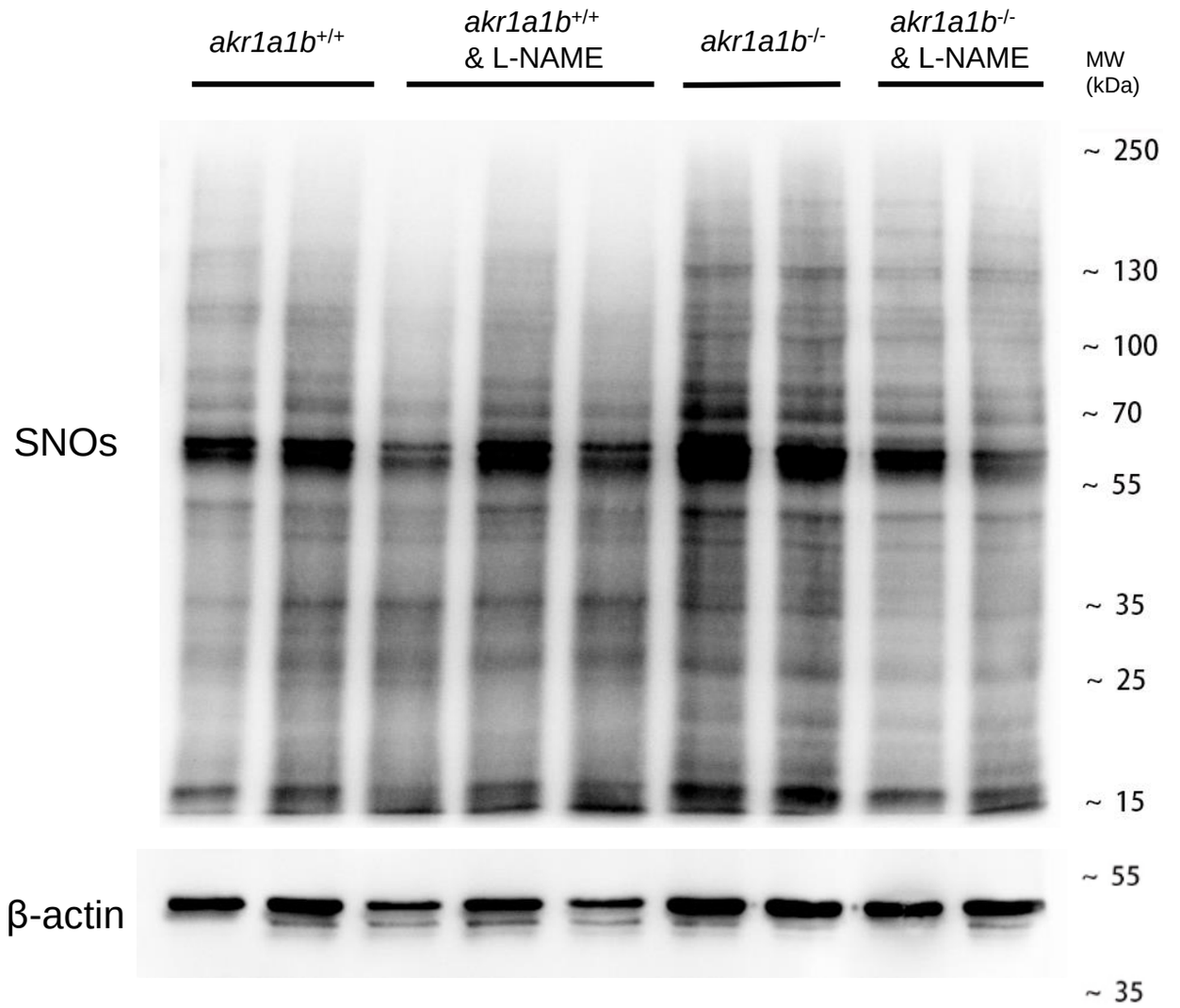

Supplement Figure 7: L-NAME treatment reduced S-nitrosylated proteins in 96 hpf Δ-23 *akr1a1b*$^{-/-}$ larvae, related to Figure 7

Western blot shows increased S-nitrosylated proteins (SNOs) in 96 hpf *akr1a1b*$^{-/-}$ larvae, which was prevented by 20 µM L-NAME treatment.

Transparent Methods

Zebrafish lines and husbandry

All experimental procedures on animals were approved by Medical Faculty Mannheim (license no.: I-19/01) and Regierungspräsidium Karlsruhe (license no. G-98/15) and carried out following the approved guidelines. Embryos/larvae of the *Tg(wt1b:EGFP)* line, where the *wt1b* promotor drives expression of EGFP (Enhanced Green Fluorescent Protein) in pronephros [(Perner et al., 2007)]; *Tg(fli1:EGFP)* line, which expresses EGFP in the vasculature under the control of the *fli1* promoter, and thus enables the visualization of the vascular system in live zebrafish[(Lawson and Weinstein, 2002)], were raised and staged as described according to hours post-fertilization (hpf)[(Kimmel et al., 1995)]. Embryos/larvae were kept in egg water at 28.5°C with 0.003 % 1-phenyl-2-thiourea (PTU, Sigma) to suppress pigmentation. Adult zebrafish were held under a 13 hours light - 11 hours dark cycle and fed with live shrimps and fish flake food. For the study both sexes were used.

Mutant generation

The CRISPR target site for *akr1a1b* was identified and selected using ZiFiT Targeter 4.1. The *akr1a1b*-CRISPR oligonucleotide, forward: 5′-TAGGTCCAAGTACTCCAGCTTC -3′, reverse: 5′-AAACGAAGCTGGAGTACTTGGA-3′, were synthesized by Sigma Aldrich. The oligonucleotides were cloned into the pT7- gRNA plasmid (Addgene). BamHI-HF (Biolabs) was used for linearization. Cas9 mRNA was synthesized from pT3TS plasmid (Addgene) after linearizing with XbaI (Biolabs). Plasmids were purified with a PCR purification kit (Qiagen). CRISPR gRNA *in vitro* transcription was done by the T7 MEGAshortscript kit and mMESSAGE MACHINE kit for Cas9 mRNA (Invitrogen). Purification of RNA after TURBO DNAse treatment was done with the MiRNeasy Mini (gRNA) and RNeasy Mini (Cas9 mRNA) kits (Qiagen). *Akr1a1b* gRNA and Cas9 mRNA (150 pg/nl) was mixed with KCl (0.1 M). The RNA mixture (1 nL) was injected directly into one-cell embryos. For genotyping, PCR-products of genomic DNA were used for Sanger sequencing (primer: forward: 5’-GGCGAGAGGATGTGTTTGTG-3’; reverse: 5’- GGGGCTCTATTATGGTCTTTTCA- 3’).

Immunohistochemistry and antibody generation

Kidney tissue from wild-type zebrafish was used for the analysis of Akr1a1b protein expression. The experiment was performed on 4 µm paraffin-embedded tissue sections fixed in 4% paraformaldehyde (PFA). The sections were dewaxed, rehydrated, antigen retrieved by

boiling sections in sodium citrate buffer (0.01 M, pH 6.0) in 480 W microwave for 20 min, followed by removal of endogenous peroxidase activity by a solution of H_2O_2/methanol (3%) for 20 min, nonspecific antibody binding was blocked by incubation with 10% FBS/PBS for 1 hour. The primary antibody diluted in 10% FBS/PBS was applied overnight at 4°C. Afterward, sections were washed three times in PBS and then incubated in a 1:1000 diluted secondary antibody for 30min at room temperature. Diaminobenzidine (DAB, SK-4100, vector laboratories) was used for chromogens for HRP and counterstained by Hematoxylin. Then all sections were dehydrated and sealed for analysis. For Akr1a1b antibody generation, peptide AWKHPDEPVLLEEPAIAAL-C was synthesized and coupled to KLH (Keyhole Limpet Hemocyanin) by PSL GmbH, Heidelberg, Germany and subsequently injected into guinea pigs for immunization following standard procedures from CF Unit Antibodies, DKFZ Heidelberg, Germany.

Western blot analysis

For analysis of Akr1a1b expression, adult zebrafish livers were taken and lysed in NP40 lysis buffer (150 mmol/L NaCl, 50 mmol/L Tris-HCl, pH 7.4, 1% NP40, 10 mmol/L EDTA, 10 % glycerol, and protease inhibitors), followed by homogenization with a syringe and incubation on ice for 30 min on a shaker. The supernatant containing the protein lysate was diluted 5:1 with Laemmli sample buffer and boiled at 95°C for 5 min, separated via SDS-PAGE, and then transferred to a nitrocellulose membrane for antibody incubation (anti-Akr 1a1b antibody 1:1000, anti-Actin antibody A2228 from Sigma-Aldrich, 1:1000), secondary HRP-conjugated antibodies 1:1000 (for β-actin: rabbit anti-goat, P0160, Dako; for Akr1a1b: goat anti-guinea pig, ABIN101281, antibodies-online.com). Visualization by enhanced chemiluminescence (ECL) was acquired after incubation with HRP (Horseradish Peroxidase) substrate.

Determination of methylglyoxal (MG), 3-Deoxyglucosone (3-DG), and glyoxal

MG, 3-DG, and glyoxal levels of zebrafish larvae, whole body lysates, and eyes were determined by LC-MS/MS, as described previously[(Zhou et al., 2019)]. Tissue MG levels were determined by derivatization with 1,2-diaminobenzene (DB). Briefly, pre-weighed amounts of tissue (10 mg) were homogenized in ice-cold 20 % (wt/vol) trichloroacetic acid in 0.9 % (wt/vol) sodium chloride (20 µL) and water (80 µL). An aliquot (5 µL) of the internal standard (13C3-MG; 400 nM) was then added, and the samples mixed. Following centrifugation (20,817 g; 5 minutes at 4°C), 35 µL of the supernatant was transferred to an HPLC vial containing a 200-µL glass interest. An aliquot (5 µL) of 3% sodium azide (wt/vol) was then added to each sample, followed by 10 µL of 0.5 mM DB in 200 mM HCl containing 0.5 mM diethylenetriaminepentaacetic acid (DETAPAC) in water. The samples were then incubated for 4 hours at room temperature,

protected from the light. Samples were then analyzed by LC-MS/MS using an ACQUITY ultra-high-performance liquid chromatography system with a Xevo-TQS LC-MS/MS mass spectrometer (Waters). The columns were a Waters BEH C18 (100 × 2.1 mm) and a guard column (5 × 2.1 mm). The mobile phase was 0.1% formic acid in water with a linear gradient of 0% to 100% 0.1% formic acid in 50% acetonitrile/water over 0 to 10 minutes; the flow rate was 0.2 mL/min and the column temperature was 5°C. The capillary voltage was 0.5 kV, the cone voltage 20 V, the interscan delay time 100 ms, the source and desolvation gas temperatures 150°C and 350°C, respectively, and the cone gas and desolvation gas flows were 150 and 800 L/h, respectively. Mass transitions (parent ion → fragment ion; collision energy), retention time, the limit of detection, and recoveries were as follows: 145.0 → 77.1, 24eV, 5.93 minutes, 0.52 pmol, and 98%.

Determination of activity of Akr, ALDH and Glo1 enzymes

Akr activity was determined spectrophotometrically by measuring the rate of reduction of NADPH at 340 nm at pH 7.0 at 25°C. The assay mixture contained potassium phosphate (100 mM), methylglyoxal (MG, 0.1–2 mM) and NADPH (0.1 mM). One unit of enzyme activity is defined as the amount of the enzyme required to oxidize 1 μmol of NADPH/min. Glo1 activity measurement was based upon the formation of S-D-lactoylglutathione from the hemithioacetal substrate, prepared from the pre-incubation of sodium phosphate (50 mM, pH 6.6), methylglyoxal (2 mM) and reduced GSH (2 mM), and was determined spectrophotometrically by measuring the increase in absorbance at 235 nm at pH 6.6 at 25°C. ALDH activity was assayed at 25°C in 75 mM Tris-HCl (pH 7.6) containing BSA (10 mM), NADP (0.5 mM), and MG (0.1–2 mM).

Microscopy and analysis of pronephric alteration

For *in vivo* imaging of pronephric structures of embryos, 48 hpf *Tg(wt1b:EGFP)* embryos were anesthetized with tricaine (0.003%) and mounted in low melting point agarose (Promega, 1 %) dorsally. Images were taken by Leica DFC420 C camera, attached to a Leica MZ10 F modular stereo microscope. Alterations of the pronephros were quantified by measuring the size of glomerular length, width, and neck length using Leica LAS V4.8 software.

Determination of pronephros function

After 72 hpf, Texas-Red® tagged 70 kDa dextran (3 nl, 2 mg/ml in PBS) was injected into the sinus venous of larvae. Images of living fish were taken sequentially at approximately 1, 24, and 48 hours post-injection (hpi) using an inverted microscope (Leica DMI 6000B) with a camera

(Leica DFC420 C) and the Leica LAS application suite 3.8 software. NIH's ImageJ application was used to measure maximum fluorescence density in the heart area. The fluorescence values at 24 hpi and 48 hpi were divided by the fluorescence values of 1hpi; respectively, for each fish, the result was shown as a ratio of the fluorescence values[(Sharma et al., 2016)].

Analysis of kidney and liver morphology

For organ preparations, adult zebrafish were euthanized with tricaine (250 mg/L) until the operculum movement stopped entirely. The fish were decapitated behind the operculum then transferred into pre-cooled 1 × PBS. Livers and kidneys, which remained in the body, were fixed in 10 % buffered formalin, removed, routinely embedded in paraffin, and cut into 4 µm-thick sections for hematoxylin and eosin staining and for Periodic acid-Schiff reaction, partly in combination with diastase. All stainings were carried out according to standard protocols. Kidneys for EM study were fixed in 2 % glutaraldehyde/0.01 M Na-cacodylate buffer and further processed according to protocols of the Electron Microscopy Core Facility of Heidelberg University. For quantification of PAS-positive hyaline droplets on EM sections we have analyzed up to 20 images per genotype according to the following criteria: 0 = absent (a few small droplets in single tubulus sections were ignored and scored as "zero"), + = small and ++ = medium.

Detection of S-Nitrosylation

S-Nitrosylation was detected by using the Biotin Switch Assay Kit (Abcam, ab236207), with a modification of the "Biotin-Switch" method[(Jaffrey and Snyder, 2001)], according to the manufacturer's instructions to measure S-nitrosylated (S-NO) proteins in larval and adult lysates. Inhibition of S-Nitrosylation was achieved by L-NAME treatment (N5751-1G; Sigma-Aldrich).

Measurement of adult zebrafish blood glucose

Adult zebrafish were transferred to single boxes the day before. The next day, the fish were either directly euthanized for blood sugar measurements under overnight fasting conditions or fed with flake food (0.5 g) for postprandial conditions. After feeding, the zebrafish were euthanized in tricaine (250 mg/L), and blood glucose was measured[(Wiggenhauser et al., 2020)].

Metabolite analysis by GC/MS and UPLC-FLR

Detection was done in cooperation with the Metabolomics Core Technology Platform from the Centre of Organismal Studies Heidelberg. At 96 hpf, zebrafish larvae were anesthetized with tricaine (0.003%), collected, and snap-frozen in liquid nitrogen. Metabolites were

determined via semi-targeted gas chromatography-mass spectrometry (GC/MS) analysis and ultra-performance liquid chromatography with fluorescence detection (UPLC-FLR) analysis (67). Frozen, ground sample material from zebrafish was extracted in 100% MeOH (360 µL) for 15 minutes at 70°C with vigorous shaking. As internal standards, ribitol (20 µL, 0.2 mg/mL) and heptadecanoic acid (10 µL, 0.2 mg/mL) were added to each sample. After the addition of chloroform (200 µL), samples were shaken at 37°C for 5 minutes. To separate polar and organic phases, water (400 µL) was added, and samples were centrifuged for 10 min at 11,000 × g. For the derivatization, the polar (upper, 700 µL) phase was transferred to a fresh tube and dried in a speed-vac (vacuum concentrator) without heating. Pellets of the aqueous phase after extraction were re-dissolved in methoximation (20 µL) reagent containing methoxyamine hydrochloride (20 mg/mL, Sigma-Aldrich 226904) in pyridine (Sigma-Aldrich 270970) and incubated for 2 hours at 37°C with shaking. For silylation, N-methyl-N-(trimethylsilyl) trifluoroacetamide (MSTFA, 32.2 µL, Sigma M7891) and Alkane Standard Mixture (2.8 µL, 50 mg/mL C10–C40; Fluka 68281) were added to each sample. After incubation for 30 min at 37°C, samples were transferred to glass vials for GC/MS analysis. To analyze total fatty acids, the lower organic phase (chloroform, 150 µL) after extraction were transferred to a fresh reaction tube (1.5 mL) and dried in a speed-vac without heating. For transmethylation reactions, pellets were re-dissolved in TBME (tert-butyl methyl ether, 40 µL, Sigma-Aldrich) and TMSH (trimethylsulfoniumhydroxid, 20 µL, Sigma-Aldrich), incubated for 45 minutes at 50°C, and transferred to glass vials for GC/MS analysis of the fatty acid methyl esters (FAMEs). A GC/MS-QP2010 Plus (Shimadzu) fitted with a Zebron ZB 5MS column (Phenomenex; 30 meter × 0.25 mm × 0.25 µm) was used for GC/MS analysis. The GC was operated with an injection temperature of 230°C and a 1 µL sample was injected with split mode (1:10). The GC temperature program started with a 1 min hold at 40°C followed by a 6°C/min ramp to 210°C, a 20°C/min ramp to 330°C, and a bake-out for 5 min at 330°C using Helium as carrier gas with constant linear velocity. The MS was operated with ion source and interface temperatures of 250°C, a solvent cut time of 7 minutes, and a scan range (m/z) of 40 to 700 with an event time of 0.2 s. The “GCMS solution” software (Shimadzu) was used for data processing.

Incubation experiments with glutamate and alanine

Fertilized eggs were incubated at 28.5°C in 6 well plates with 5 ml solutions that was changed daily. The solution contained egg water, glutamate (0.1 and 1 mM), alanine (1 and 5 mM) and PTU (0.003%). Embryos were raised until 48 hpf and analyzed for pronephric structure.

Real time quantitative PCR analysis

Expression of *akr1a1b* gene and cytosolic phosphoenolpyruvate carboxykinase (cPEPCK) in embryos/larvae and in different organs of adult zebrafish were analyzed by RT-qPCR technology. All organs were dissected from adult zebrafish under either over-night fasting or postprandial conditions. Total RNA was isolated using the RNeasyMini-Kit (QiagenTM, 74104) following the manufacturer's protocol. First-strand cDNA was synthesized from the total RNA using the cDNA Synthesis Kit (ThermoFisher Scientific, K1671). *Akr1a1b* gene expression in embryos/larvae was normalized to *β-actin*, and cPEPCK expression was normalized to *Beta-2 microglobulin* (*b2m*). All primers for RT-qPCR are shown in table 1.

Measurement of glutamate and alanine in adult zebrafish kidneys and livers

Glutamate and alanine concentration was measured using the Glutamate Assay Kit (MAK004, Sigma-Aldrich) and Alanine Assay Kit (MAK001, Sigma-Aldrich) according to the manufacturer's instructions, and represented as ng/mg tissue.

Statistics

All data are presented as mean ± SD. Statistical significance between two groups was analyzed using two-tailed Student's *t*-test using GraphPad Prism, For comparisons among more than two groups, one-way or two-way ANOVA followed by appropriate multiple comparison tests was used. *P* value less than 0.05 was considered significant.

References for Supplements

Jaffrey, S.R., and Snyder, S.H. (2001). The biotin switch method for the detection of S-nitrosylated proteins. Sci STKE *2001*, pl1.

Kimmel, C.B., Ballard, W.W., Kimmel, S.R., Ullmann, B., and Schilling, T.F. (1995). Stages of embryonic development of the zebrafish. Dev Dyn *203*, 253-310.

Lawson, N.D., and Weinstein, B.M. (2002). In vivo imaging of embryonic vascular development using transgenic zebrafish. Dev Biol *248*, 307-318.

Perner, B., Englert, C., and Bollig, F. (2007). The Wilms tumor genes wt1a and wt1b control different steps during formation of the zebrafish pronephros. Dev Biol *309*, 87-96.

Sharma, K.R., Heckler, K., Stoll, S.J., Hillebrands, J.L., Kynast, K., Herpel, E., Porubsky, S., Elger, M., Hadaschik, B., Bieback, K.*, et al.* (2016). ELMO1 protects renal structure and ultrafiltration in kidney development and under diabetic conditions. Sci Rep *6*, 37172.

Wiggenhauser, L.M., Qi, H., Stoll, S.J., Metzger, L., Bennewitz, K., Poschet, G., Krenning, G., Hillebrands, J.L., Hammes, H.P., and Kroll, J. (2020). Activation of Retinal Angiogenesis in Hyperglycemic pdx1 (-/-) Zebrafish Mutants. Diabetes *69*, 1020-1031.

Zhou, H.L., Zhang, R., Anand, P., Stomberski, C.T., Qian, Z., Hausladen, A., Wang, L., Rhee, E.P., Parikh, S.M., Karumanchi, S.A.*, et al.* (2019). Metabolic reprogramming by the S-nitroso-CoA reductase system protects against kidney injury. Nature *565*, 96-100.